Circulation

ORIGINAL RESEARCH ARTICLE

ALDH2/eIF3E Interaction Modulates Protein Translation Critical for Cardiomyocyte Ferroptosis in Acute Myocardial Ischemia Injury

Xin Chen, PhD*; Xiujian Yu, PhD*; Shanshan Zhong, PhD*; Ping Sha, PhD; Rui Li, PhD; Xiaodong Xu, PhD; Ningning Liang, PhD; Lili Zhang, PhD; Luxiao Li, PhD; Jingyu Zhang, MD, PhD; Mingyao Zhou, MS; Tongwei Lv, MD, PhD; Haoran Ma, PhD; Yongqiang Wang, PhD; Yanwen Ye, PhD; Chunzhao Yin, PhD; Shiting Chen, BS; Jinwei Tian, MD, PhD; Aijun Sun, MD, PhD; Weiyuan Wang, MD, PhD; Dewen Yan, MD, PhD; Huang-Tian Yang, MD, PhD†; Hui Huang, MD, PhD†; Pan Li, MD, PhD†; Huiyong Yin, PhD†

BACKGROUND: As an iron-dependent form of regulated cell death caused by lipid peroxidation, ferroptosis has been implicated in ischemic injury, but the underlying mechanisms in acute myocardial infarction (AMI) remain poorly defined. ALDH2 (acetaldehyde dehydrogenase 2) catalyzes detoxification of lipid aldehydes derived from lipid peroxidation and acetaldehydes from alcohol consumption. The Glu504Lys polymorphism of ALDH2 (rs671, ALDH2*2), affecting ≈40% of East Asians, is associated with increased risk of myocardial infarction (MI). This study aims to investigate the role of ALDH2*2 and ferroptosis in AMI.

METHODS: A Chinese cohort of 177 patients with acute heart failure with ALDH2 wild type and ALDH2*2 was enrolled. The MI mouse model of left anterior descending coronary artery ligation was conducted on wild-type and ALDH2*2 mice and mice with cardiomyocyte-specific knockdown of eIF3E (eukaryotic translation initiation factor 3 subunit E) by adeno-associated virus. The lipid peroxidation products were measured by mass spectrometry–based lipidomics and metabolomics in human plasma, mouse serum samples, mouse heart tissues, and primary cardiac myocytes.

RESULTS: Human ALDH2*2 carriers exhibit more severe heart failure after AMI with features of ferroptosis in plasma, as seen through lipidomic analysis, characterized by increased bioactive lipids and decreased antioxidants, such as coenzyme Q10 and BH4 (tetrahydrobiopterin). Similar features were observed in MI mouse models of ALDH2*2, whereas ferroptosis inhibition by Fer-1 significantly improved heart function and reversed ferroptosis markers. Importantly, ALDH2*2 significantly decreased ALDH2 protein levels, whereas ferroptosis-related markers, including TFRC (transferrin receptor) and ACSL4 (acyl-coenzyme A synthetase long-chain family member 4) were notably upregulated in the infarct heart tissues. Mechanistically, ALDH2 physically interacts with the eIF3 complex via the eIF3E factor, which prevents eIF3E-eIF4G1 (eukaryotic initiation factor 4G)-mRNA assembly. The ALDH2*2 variant causes ALDH2 deficiency, disrupting its interaction with the eIF3 complex by releasing the bound eIF3E to assemble an eIF3E-eIF4G1-mRNA ternary complex, thereby driving selective translation of mRNAs (eg, TFRC, ACSL4, and UAP1) containing the GAGGACR (R represents A/G) motif to promote ferroptosis. Consistently, cardiomyocyte-specific eIF3E knockdown restored ALDH2*2 cardiac function by attenuating ferroptosis in MI.

CONCLUSIONS: ALDH2*2 aggravates acute heart failure after MI by promoting the selective translation of mRNAs containing the GAGGACR motif, thereby driving cardiomyocyte ferroptosis. Targeting ferroptosis represents a potential therapeutic option for mitigating MI injury, especially for ALDH2*2 carriers.

Key Words: ALDH2 ■ eIF3E ■ ferroptosis ■ myocardial infarction ■ protein translation

Correspondence to: Huiyong Yin, PhD, Department of Biomedical Sciences, City University of Hong Kong; Shanghai Institute of Nutrition and Health, Chinese Academy of Sciences, 320 Yueyang Rd, Shanghai 200031, China, Email hyyin@sinh.ac.cn; Pan Li, MD, PhD, Department of Cardiology, Changhai Hospital, Naval Medical University, Shanghai, China, Email lipan@smmu.edu.cn; or Hui Huang, MD, PhD, Department of Cardiology, Eighth Affiliated Hospital of Sun Yat-sen University, Shennan Middle Road, Shenzhen 510275, China, Email huangh8@mail.sysu.edu.cn
*X. Chen, X. Yu, and S. Zhong contributed equally.
†H.-T. Yang, H. Huang, P. Li, and H. Yin contributed equally.
Supplemental Material is available with this article at https://www.ahajournals.org/doi/suppl/10.1161/CIRCULATIONAHA.125.075220.
For Sources of Funding and Disclosures, see page 182.

Circulation is available at www.ahajournals.org/journal/circ

Clinical Perspective

What Is New?

- The ALDH2*2 mutation aggravates acute heart failure with features of ferroptosis, including several species of elevated bioactive lipids and reduced levels of coenzyme Q10 and tetrahydrobiopterin in patient plasma.
- ALDH2 deficiency drives the preferential translation of mRNAs harboring the GAGGACR (R: A/G) motif through eIF3E-mediated ribosome remodeling, upregulating ferroptosis.
- ALDH2 directly binds to the eIF3 complex through the eIF3E factor, competitively inhibiting eIF3E-eIF4G1 assembly to control selective mRNA translation.

What Are the Clinical Implications?

- Bioactive lipids associated with ferroptosis in plasma may serve as potential markers for acute myocardial infarction patients, especially for ALDH2*2 carriers.
- Inhibiting ferroptosis emerges as a viable cardioprotective therapeutic strategy for myocardial injury, particularly for ALDH2*2 carriers.

Nonstandard Abbreviations and Acronyms

AA	arachidonic acid
AHF	acute heart failure
AMI	acute myocardial infarction
CoQ10	coenzyme Q10
CRP	C-reactive protein
CVD	cardiovascular disease
DHET	dihydroxyeicosatrienoic acid
Fer-1	ferrostatin-1
KD	knockdown
LDH	lactate dehydrogenase
MI	myocardial infarction
NC	normal control
PC	glycerophosphatidylcholine
PE	glycerophosphatidylethanolamine

Editorial, see p 185

Acute myocardial infarction (AMI) is a leading cause of death worldwide, and ischemic heart injury remains the major contributor to heart failure after AMI.[1–3] Mounting evidence has implicated various forms of cardiomyocyte cell death in ischemic injury, such as apoptosis, necroptosis, pyroptosis, and ferroptosis.[4,5] Each form of cell death plays an important role in ischemic injury, and specifically targeting different forms of cell death may have an enormous impact on developing therapeutic strategies for MI.[6]

Ferroptosis is a newly discovered form of regulated cell death primarily caused by lipid peroxidation and dysregulation of iron metabolism.[7] The TFRC (transferrin receptor) plays a critical role in iron uptake and has been regarded as a specific marker for ferroptosis.[8] Multiple reactive oxygen species (ROS) are generated from Fenton chemistry (ferric ion and hydrogen peroxide), lipoxygenases (LOX), cytochrome P450 oxidoreductase, and nicotinamide adenine dinucleotide phosphate oxidase, which attack polyunsaturated fatty acids (PUFAs) in cellular membranes. The resulting oxidized lipids are considered hallmarks of lipid peroxidation and ferroptosis.[9] On the other hand, cellular antioxidant systems, including GPX4 (glutathione peroxidase 4), Nrf2/KEAP1, ubiquinol recycling (ferroptosis suppressor protein 1, FSP1, coenzyme Q10, CoQ10), and GTP cyclohydrolase 1–mediated BH4 (tetrahydrobiopterin) production, are critical for counteracting lipid peroxidation, which precedes ferroptosis.[10] ACSL4 (acyl-CoA synthetase long-chain family member 4) plays an important role in incorporating PUFAs into cellular membranes under ferroptosis conditions.[11] ACSL4 also preferentially activates arachidonic acid (AA) and adrenic acid (AdA) by esterifying them into AA-CoA and AdA-CoA as key ferroptotic signals while also modulating prostaglandin E_2 secretion.[12] Mounting evidence from the past decade has implicated ferroptosis in various human diseases, especially ischemia/reperfusion (I/R) injury. However, the underlying mechanisms of ferroptosis in AMI remain poorly defined.[13]

ALDH2 (aldehyde dehydrogenase 2) is a critical enzyme that catalyzes the oxidation of acetaldehydes from alcohol or endogenous lipid aldehydes resulting from lipid peroxidation.[14] A loss-of-function single-nucleotide polymorphism in the ALDH2 gene, ALDH2*2 (or ALDH2 rs671), affects ≈30% to 50% of the East Asian population, has been linked to an increased risk of MI and other cardiovascular diseases (CVD).[15,16] Most previous studies have attributed the increased risk of CVD in ALDH2*2 carriers to the accumulation of aldehydes as a result of the significantly decreased enzymatic function of ALDH2.[17,18] We and others have discovered multiple nonenzymatic functions of ALDH2 in the pathogenesis of CVD.[15,19,20] However, it remains unknown whether ALDH2 regulates lipid peroxidation and the ferroptosis pathway in MI.[21,22]

In this study, we discovered a novel mechanism by which ALDH2 physically interacts with the eIF3 complex via the eIF3E factor, thereby preventing eIF3E from binding to eIF4G1 (eukaryotic initiation factor 4G). The ALDH2*2 variant leads to ALDH2 deficiency, disrupting its interaction with the eIF3 complex and releasing the bound eIF3E to assemble an eIF3E-eIF4G1-mRNA ternary complex. This process promotes the selective

translation of mRNAs (eg, TFRC, ACSL4, and UAP1) containing the GAGGACR (R: A/G) motif, ultimately promoting ferroptosis. Conversely, eIF3E knockdown (KD) or ferroptosis inhibition using ferrostatin 1 (Fer-1) attenuates heart failure in ALDH2*2 mice. These findings suggest that inhibiting ferroptosis could serve as a novel therapeutic strategy for ischemic heart injury.

METHODS

All supporting data are available within the article and its Supplemental Material. All data, protocols, and study materials are available to other researchers to reproduce the results. Ribosome profiling (Ribo-seq) raw data were uploaded to the Gene Expression Omnibus (www.ncbi.nlm.nih.gov/geo) under accession number GSE305516. Liquid chromatography-tandem mass spectrometry raw data were deposited as Mendeley Data V1 (doi:10.17632/h273n9twh6.1). The detailed methods used in this study are provided in the Supplemental Material.

Experimental Animals and Myocardial Infarction Model

Male C57BL/6J and ALDH2*2 knockin (rs671 variant) mice were maintained under specific pathogen–free conditions with ad libitum access to irradiated normal chow and water (animal approval Nos. SINH-2021-YYH-1 and SINH-2022-YYH-1). All procedures conformed to institutional ethics guidelines and were approved by the animal care and use committee of the Shanghai Institute of Nutrition and Health, Chinese Academy of Sciences. To minimize hormonal fluctuations, we only used male mice in the animal experiments. Male C57BL/6J, and male ALDH2*2 knockin mice that were generously provided by Dr Yong Cang's laboratory at ShanghaiTech University[23] were used for all echocardiography and survival analyses. Anesthesia was induced with isoflurane inhalation, followed by mechanical ventilation with a volume-regulated SAR-830/AP small animal ventilator (CWE Inc, Ardmore, PA). A preemptive dose of carprofen (2 mg/kg IP; MedChemExpress, HY-B1227) was administered before surgery. No postoperative analgesics were given to avoid confounding effects on serum metabolite profiling. Body temperature was maintained at 37 C throughout the procedure. Mice were randomly selected for either sham or MI induction groups. MI was produced by permanently ligating the left anterior descending coronary artery with 7-0 Prolene suture. In sham-operated mice, the suture was placed but not tightened to occlude the artery. The chest was then closed over the exteriorized suture ends with 5-0 Prolene suture, and mice were returned to the rearing cage for recovery and feeding. Either vehicle (1% dimethyl sulfoxide DMSO in 0.9% saline IP) or Fer-1 (10 mg/kg in 0.9% saline IP) was administered twice, 24 hours and 2 hours before ischemia induction.

Human Peripheral Blood Samples and Left Ventricular Tissues

All clinical parameters (Table) were recorded upon admission of ST-segment–elevation MI (STEMI) patients before any surgical intervention. Sample collection followed standardized protocols for all participants, minimizing temporal variability. Peripheral blood samples from 177 patients with STEMI were collected under Changhai Hospital ethics committee–approved protocols. Genotyping identified 52 (29%) ALDH2*2 heterozygotes and 14 (8%) homozygotes. Cardiac injury biomarkers (BNP [brain natriuretic peptide], CRP [C-reactive protein], and LDH [lactate dehydrogenase]) were compared between wild-type (WT) and ALDH2*2 carriers. ALDH2*2 heterozygotes showed significantly elevated BNP, CRP, and LDH levels compared with ALDH2*1 homozygotes (Table S5). ALDH2*2 homozygotes showed no significant change, potentially because of limited sample size. Given this, heterozygous and homozygous carriers were combined for subsequent analyses (Table). Given the acute biomarker elevations, we prioritized investigating immediate MI injury and did not collect long-term follow-up data. Additionally, left ventricular tissues were obtained from 3 patients with end-stage dilated cardiomyopathy undergoing heart transplantation at Changhai Hospital. The characteristics of these 3 patients are outlined in Table S1. All procedures involving human participants, including the collection of plasma and tissue samples, were carried out in strict accordance with the ethical standards established by the institutional research committee (ethics committee of Changhai Hospital of Shanghai, Shanghai, China; approval No. CHEC2024-320). Written informed consent was obtained from all participants or their legally authorized representatives before the initiation of sample collection.

Statistical Analysis

All mice were randomly assigned to groups before the experiments. Experiments, including cell, animal, and human experiments, were analyzed using a 2-tailed Student *t* test for normally distributed data and a Mann-Whitney test for non-normally distributed data by using GraphPad Prism 9.0 software. A 1-way or 2-way ANOVA was performed for comparisons between multiple groups, followed by Tukey's multiple comparisons after the test. All data are reported as the mean±SEM or the mean±SD from at least 3 independent experiments. Statistical significance was determined at $P<0.05$, with significance levels indicated as $^{*}P<0.05$, $^{**}P<0.01$, and $^{***}P<0.001$.

RESULTS

ALDH2*2 Is Positively Associated With Severity of Acute Heart Failure After MI

To explore the roles of ALDH2 in acute heart failure (AHF) induced by MI, we enrolled a cohort of 177 patients with STEMI with elevated BNP levels (>100 pg/mL), a diagnostic marker for AHF.[24] The clinical characteristics of all of these patients are summarized in the Table. Blood cells were used for ALDH2 genotyping, and plasma samples were used for targeted metabolomics (Figure 1A). The patients were genotyped for ALDH2*1 (WT, n=111, 62.7%) and ALDH2*2 (hetero/homozygous, n=66, 37.3%; Figure 1A; Table). The major traditional risk factors for HF between these 2 groups showed no intergroup differences, including age, sex, BMI, lipid profiles (total cholesterol, triglycerides, low-density

Table. Clinical Characteristics of Human Samples From AHF Patients After Myocardial Infarction

Variables	ALDH2*1 (WT) (n=111)	ALDH2*2 (variant) (n=66)	*P* value
Age, y	65.3±12.0	66.4±12.2	0.468
Sex (male), n (%)	91 (81.1)	59 (89.4)	0.210
BMI, kg/m^2	24.9±3.4	25.5±4.2	0.511
TC, mmol/L	4.8 (4.0, 5.4)	4.7 (4.1, 5.4)	0.907
TG, mmol/L	1.5 (1.1, 2.2)	1.2 (1.0, 1.7)	0.051
LDL-C, mmol/L	3.1 (2.3, 3.7)	3.1 (2.4, 3.7)	0.675
HDL-C, mmol/L	1.1 (1.0, 1.3)	1.2 (1.0, 1.3)	0.514
Cigarette smoking, n (%)	52 (46.4)	32 (48.5)	0.956
Hypertension, n (%)	59 (53.2)	34 (51.5)	0.956
Diabetes, n (%)	37 (33.3)	22 (33.3)	1.000
Family history of CVD, n (%)	13 (11.7)	6 (9.1)	0.769
Alcohol habit, n (%)	30 (27.0)	7 (10.6)	0.016*
LDH, U/L	426.5 (283.5, 779.5)	615.5 (381.0, 972.5)	0.013*
cTnI, ng/mL	15.3 (4.6, 25.6)	25.1 (5.9, 26.5)	0.192
BNP, pg/mL	310.3 (189.7, 476.0)	392.7 (247.0, 600.1)	0.035*
CRP, mg/L	1.3 (0.5, 7.0)	2.2 (0.5, 15.7)	0.039*
EF (%)	59.0 (56.0, 63.0)	53.0 (49.8, 58.0)	<0.0001*
FS (%)	32.0 (29.0, 34.0)	28.0 (25.0, 32.0)	0.0005*
IVS, cm	1.1 (1.0, 1.2)	1.1 (1.0, 1.2)	0.553
LVESD, cm	3.2 (2.9, 4.2)	3.5 (3.1, 4.0)	0.147
LVEDD, cm	4.4 (4.0, 4.8)	4.8 (4.3, 5.2)	<0.0001*

Continuous variables are presented as mean±SD when normally distributed (per Shapiro-Wilk test) or as median and interquartile range when skewed or contain outliers. Categorical variables are reported as count (n) and percentage (%). *P* values are 2 tailed and derived from Mann-Whitney *U* tests for continuous variables and χ^2 tests for categorical variables, comparing ALDH2*2 with WT. ALDH2 indicates aldehyde dehydrogenase 2; ALDH2*1, wild-type; ALDH2*2, variant ALDH2 genotype; BMI, body mass index; BNP, brain natriuretic peptide; CRP, C-reactive protein; cTnI, cardiac troponin I; CVD, cardiovascular disease; EF, ejection fraction; FS, fraction shortening; HDL-C, high-density lipoprotein cholesterol; IVS, interventricular septal; LDH, lactate dehydrogenase; LDL-C, low-density lipoprotein cholesterol; LVEDD, left ventricular end-diastolic diameter; LVESD, left ventricular end-systolic dimension; TC, total cholesterol; and TG, triglyceride.

*P values (P<0.05) denote statistical significance.

lipoprotein cholesterol, and high-density lipoprotein cholesterol), smoking, hypertension, diabetes, and family history of CVD. Interestingly, the prevalence of drinking was lower in ALDH2*2 than in the WT (Table), consistent with previous reports. However, ALDH2*2 carriers demonstrated elevated injury markers (higher LDH, BNP, and CRP), though cardiac troponin I levels were comparable. On the other hand, heart function deteriorated more in the ALDH2*2 variant than in the WT, evidenced by significant reductions in ejection fraction and fraction shortening, along with an increased left ventricular end-diastolic volume. No significant changes were observed in interventricular septal thickness or left ventricular end-systolic dimension (Table). These findings suggest that the ALDH2*2 variant is associated with more severe AHF after MI, independent of alcohol consumption or traditional risk factors.

Taken together, ALDH2*2 carriers manifest aggravated AHF after MI, independent of alcohol consumption, likely because of impaired ALDH2-mediated cytoprotective pathways rather than traditional risk factors.

Targeted Metabolomic Analysis Identified Features of Ferroptosis in the Plasma of Patients With ALDH2*2 AHF After MI

ALDH2 is a key enzyme in detoxifying ethanol-derived acetaldehyde and endogenous lipid aldehydes generated from lipid peroxidation,[25] processes closely linked to ferroptosis.[26] However, it remains unknown whether ferroptosis-driven lipid peroxidation exacerbates AHF in ALDH2*2 carriers after MI. To address this, we performed mass spectrometry–based targeted oxidative lipidomics and metabolomics on patient plasma samples. We observed a general trend of elevated levels of multiple oxidized phospholipids in plasma samples of patients with ALDH2*2, although they did not reach statistical significance after false discovery rate correction (Figure 1A and 1B). However, specific bioactive lipids derived from oxidized lipids, free AA (20:4 n-6), and 15-deoxy-$\Delta_{12,14}$-prostaglandin D_2 (15d-PGD_2), were markedly elevated in patients with ALDH2*2 (Figure 1C). AA provides the substrate for ACSL4-mediated esterification into peroxidation-prone

ORIGINAL RESEARCH ARTICLE

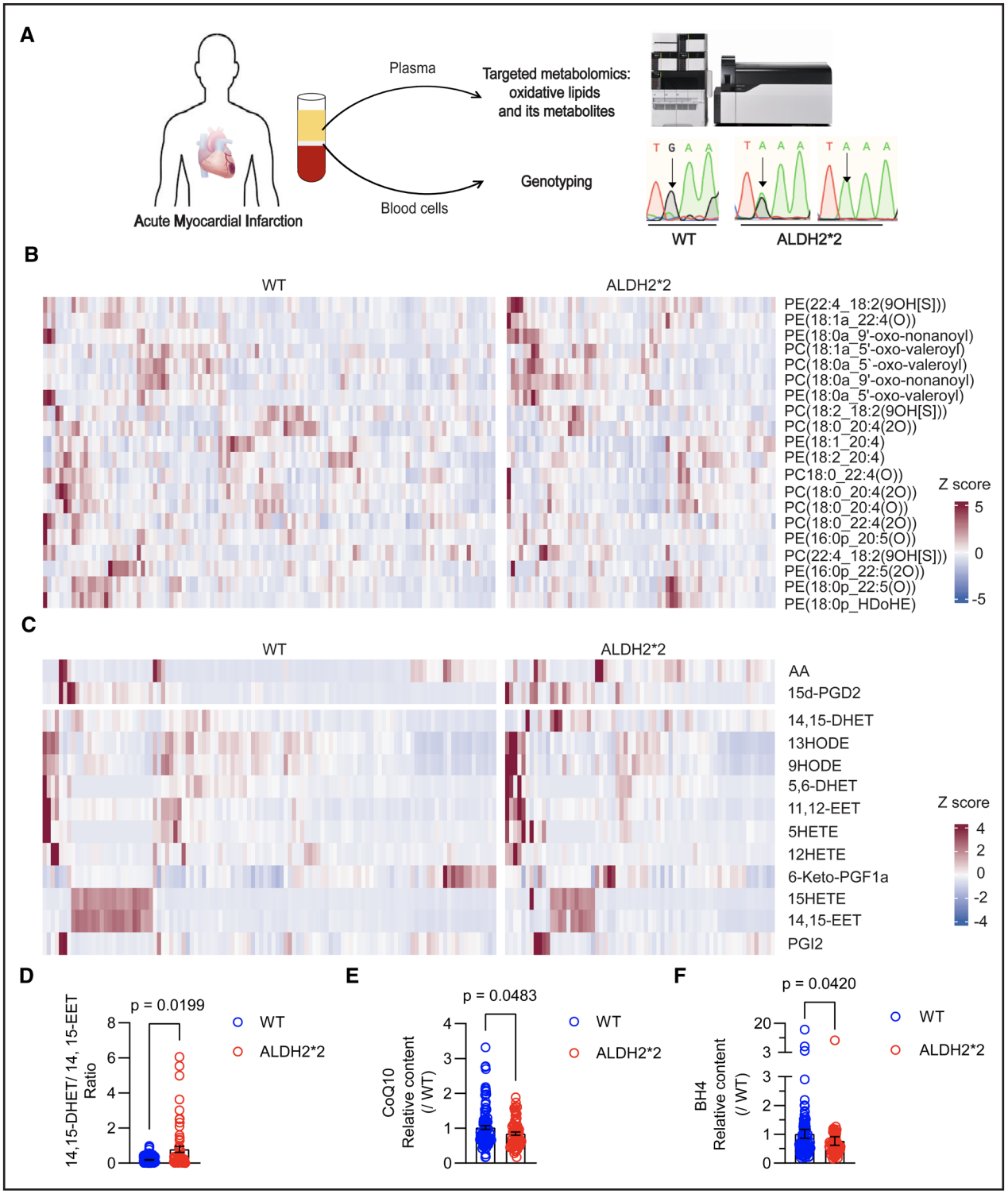

Figure 1. Targeted metabolomic analysis of oxidative lipids and related metabolites in the human plasma samples from ALDH2 WT and ALDH2*2 carriers.

A, Experimental design. A BNP (brain natriuretic peptide) level >100 pg/mL was classified as heart failure. ALDH2 (acetaldehyde dehydrogenase 2) genotypes were confirmed by direct sequencing of PCR-amplified genomic DNA, categorizing patients into two groups: wild type (WT; G/G, n=111) and ALDH2*2 carriers (G/A and A/A, n=66). **B** and **C**, Relative oxidized phospholipids levels (**B**) and relative bioactive lipids levels (**C**) in the plasma of WT patients and patients with ALDH2*2. Each metabolite was adjusted to internal standards. Upregulation, red; downregulation, blue. The color scale represents the *Z* score. AA, adjusted $P<0.0001$; 15d-PGD_2, adjusted $P=0.0401$. **D**, 14,15-dihydroxyeicosatrienoic acid (DHET)/14,15-epoxyeicosatrienoic acid (EET) ratio. **E** and **F**, Relative coenzyme Q10 (CoQ10) content (**E**) and relative BH4 content (**F**) in the plasma of WT patients and patients with ALDH2*2 from **A**. Data are presented as mean±SEM. Statistical analysis was performed using a Mann-Whitney *U* test with multiple testing. AA indicates arachidonic acid; BH4, tetrahydrobiopterin; PC, phosphatidylcholine; PCR, polymerase chain reaction; PE, phosphatidylethanolamine; and WT, wild-type.

phospholipids (AA-phosphatidylethanolamine [PE]/AdA-PE), which are subsequently oxidized by LOXs during ferroptosis.[12] 15d-PGD_2, a downstream cyclooxygenase-derived product of PGD_2 from AA, contributes to inflammation and oxidative stress.[27] Additionally, the 14, 15-dihydroxyeicosatrienoic acid (DHET)/14,15-epoxy eicosatetraenoic acid (products from the P450 pathway in AA metabolism) ratio, a validated predictor of 1-year heart failure mortality and also downstream metabolites of AA,[28] was significantly elevated in ALDH2*2 plasma (Figure 1C and 1D). Collectively, these findings suggest that ferroptosis-related lipid peroxidation is activated in patients with ALDH2*2 with AHF after MI. Moreover, the levels of 2 important antioxidants, CoQ10 and BH4, were significantly decreased in the plasma of patients with ALDH2*2 (Figure 1E and 1F). Noteworthy, both CoQ10 and BH4 are closely correlated with heart failure and the ferroptosis pathway,[26,29] further supporting ferroptosis induction in patients with ALDH2*2.

Together, elevated bioactive lipid levels alongside decreased BH4 and CoQ10 in the plasma of patients with ALDH2*2 strongly suggest that ALDH2*2-mediated lipid peroxidation is closely linked to ferroptosis in AHF after MI.

ALDH2 *2 Mice Showed Worse Heart Function in the MI Model

To further confirm that ALDH2*2 exacerbates AHF after MI through ferroptosis pathways, we employed an MI mouse model by ligating the left anterior descending coronary artery. Echocardiography was performed at the indicated time points (Figure S1A and S1B). The first 4 days after MI represent the acute inflammatory phase, characterized by intense infiltration of inflammatory cells.[30] Heart function deteriorated more in ALDH2*2 mice, as indicated by consistently lower left ventricular ejection fraction (LVEF) and left ventricular fractional shortening (LVFS) throughout the experiment period (Figure S1A and S1B). These findings suggest that the ALDH2*2 mutant exacerbates cardiac dysfunction since the acute inflammatory phase after MI. When we set 3 days after MI as the AMI stage, ALDH2*2 mice exhibited significant upregulation of heart injury makers, including *Myh7* and *Nppa* mRNA in infarct tissues (Figure S1C). Additionally, the levels of mitochondrial damage–associated molecular patterns, including mt-16S rRNA and mt-ND4,[31] were considerably higher in the serum of ALDH2*2 mice (Figure S1D). These results align with clinical observations that the ALDH2*2 variant is associated with exacerbated AHF after MI.

Leukocytes ($CD45^+$; Figure S2A through S2C) and neutrophils ($CD11b^+Ly6G^+Ly6C^-$; Figure S2A, S2B, and S2D) were significantly elevated in the blood of ALDH2*2 mice on day 3 after MI, indicating an amplified acute inflammatory response. In contrast, monocytes ($CD11b^+Ly6G^-Ly6C^+$) remained unchanged (Figure S2A, S2B, and S2E), suggesting heightened neutrophil-driven inflammation in ALDH2*2 mice on day 3 after MI.

Taken together, the ALDH2*2 mutant exacerbates AHF after MI, driven by heightened cardiac injury, mitochondrial damage, and neutrophil-mediated inflammation during the acute inflammatory phase. These findings are consistent with observations in patients that link the ALDH2*2 variant to worse AHF after MI.

Ferroptosis Was Involved in AHF in ALDH2*2 Mice and Inhibition of Ferroptosis Improved Heart Function

We next performed untargeted metabolomics on serum samples from mice on day 3 after MI. ALDH2*2 mice exhibited elevated levels of several bioactive lipids, including linoleic acid derivatives (9-hydroxyoctadecadienoic acid [9-HODE], 13-hydroxyoctdecadienoic acid [13-HODE], 10-hydroxydocosahexaenoic acid [10-HDoHE], and PE [18:0_9-HODE]), PUFAs (PG36:3, docosapentaenoic acid [DPA], and docosahexaenoic acid [DHA]), monohydroxy fatty acids (12-hydroxyeicosapentaenoic acid [12-HEPE]), and saturated lipids (Lyso PE17:0), compared with WT mice (Figure 2A). Corticosterone, a known marker of MI injury,[32] was increased. At the same time, cardioprotective metabolites, including propionyl-L-carnitine and N-acetyl-L-methionine,[33] were significantly reduced in ALDH2*2 mice (Figure 2A). However, glutathione was upregulated in ALDH2*2 mice (Figure 2A), likely as a compensatory response to oxidative stress, but appeared to be insufficient to prevent cardiac injury. Pathway enrichment analysis highlighted AA metabolism, biosynthesis of unsaturated fatty acids, linoleic acid metabolism, and ROS–related pathways as well as the ferroptosis pathway, which were significantly enriched in ALDH2*2 mice compared with WT controls (Figure 2B). These findings suggest that ferroptosis plays a critical role in ALDH2*2-mediated exacerbation of AHF after MI.

Then, we pretreated mice with the ferroptosis inhibitor Fer-1 or vehicle before MI surgery (Figure S3A), as described in a previous study.[34] Baseline LVEF, LVFS, and body weight were equivalent across groups (Figure S3B through S3D). No significant differences were observed in 28-day body weight (Figure S3E) and survival rates (Figure S3F) between WT and ALDH2*2 mice after MI, regardless of Fer-1 pretreatment. Interestingly, compared with WT controls, vehicle-pretreated ALDH2*2 mice exhibited greater impaired cardiac function with reduced LVEF (on day 2 and day 28 after MI) and LVFS (on day 28 after MI). Fer-1 rescued both LVEF and LVFS in ALDH2*2 mice on day 2 and day 28 after MI (Table S4-1; Figure 2C and 2D). Though ineffective for WT cardiac function, Fer-1 attenuated scar size in both genotypes on day 28 after MI, with ALDH2*2 mice showing greater baseline scarring and Fer-1–mediated reduction (Figure 2C through 2F; Table S4-1 and S4-2), indicating

ORIGINAL RESEARCH ARTICLE

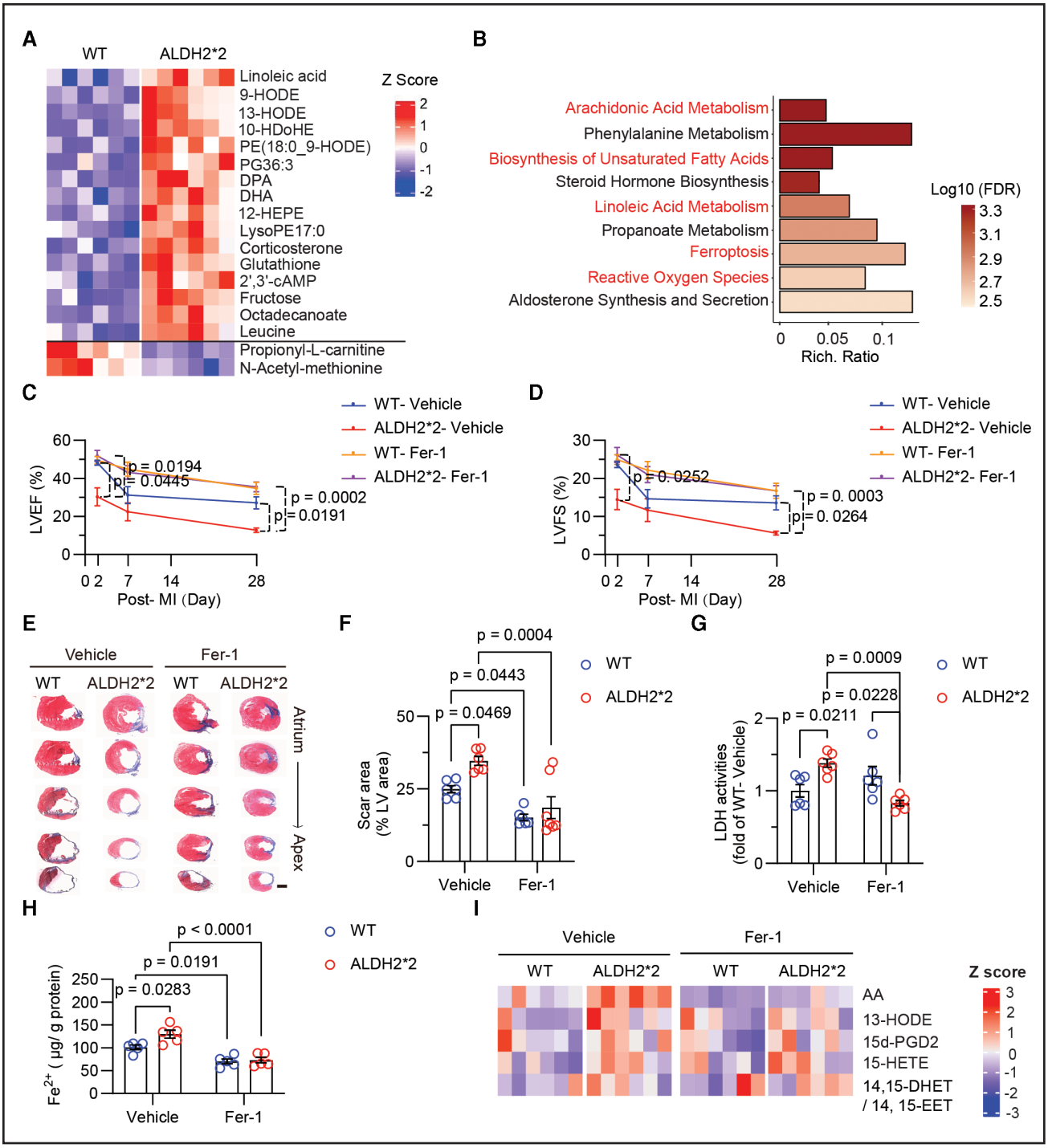

Figure 2. ALDH2*2 exacerbates acute heart failure mainly by promoting ferroptosis in mice after MI.
A and **B**, Untargeted metabolomics analysis of serum from wild-type (WT) and ALDH2*2 mice on day 3 after myocardial infarction (MI; n=6 per group). **A**, Heatmap showing significantly altered metabolites. Each row represents a specific metabolite. Upregulation, red; downregulation, blue. The color scale represents the *Z* score. **B**, Kyoto Encyclopedia of Genes and Genomes pathway enrichment of differential abundant metabolites (fold change ≥2 and false discovery rate [FDR] <0.05) in ALDH2*2 vs WT mice. Rich. Ratio is the proportion of differential metabolites mapped to a given Kyoto Encyclopedia of Genes and Genomes pathway, calculated as (No. of differential metabolites in pathway)/(total metabolites in pathway). **C** and **D**, LVEF and LVFS assessment 2, 7, and 28 days after MI in WT and ALDH2*2 mice pretreated with vehicle or ferrostatin-1 (Fer-1; n=6, 6, 6, and 7 per group). Statistical testing used 2-way ANOVA with modification for multiple comparisons. **C**, On day 2 after MI, WT- vehicle vs ALDH2*2- vehicle *P*=0.0445, ALDH2*2- Fer-1 vs ALDH2*2- vehicle *P*=0.0194; on day 28 after MI, WT- vehicle vs ALDH2*2- vehicle *P*=0.0191, ALDH2*2- Fer-1 vs ALDH2*2- vehicle *P*=0.0002; **D**, on day 2 after MI, ALDH2*2- Fer-1 vs ALDH2*2- vehicle *P*=0.0252; on day 28 after MI, WT- vehicle vs ALDH2*2- vehicle P=0.0264, ALDH2*2- Fer-1 vs ALDH2*2- vehicle *P*=0.0003. **E**, Representative Masson trichrome staining of heart sections on day 28 after MI. Scale bar=1 mm. **F**, Quantitation of infarct size in cohorts corresponding to **C** through **E**. **G**, Serum lactate dehydrogenase (LDH) activity levels on day 3 after MI (n=6 per group). **H**, Fe^{2+} content in the infarct tissues of WT (*Continued*)

Figure 2 Continued. and ALDH2*2 with vehicle or Fer-1 pretreatment on day 3 after MI (n=5 per group). **I**, Arachidonic acid (AA) and related metabolites in serum on day 3 after MI (n=6 per group). For the heatmap, data were averaged and normalized to the WT- vehicle group, with each metabolite adjusted to internal standards. Upregulation, red; downregulation, blue. The color scale represents the *Z* score. Results are reported as mean±SEM. Statistical analysis was performed using mixed-effects ANOVA with Geisser-Greenhouse correction (**C** and **D**) and 2-way ANOVA (**F** through **H**). LC-MS indicates liquid chromatography-mass spectrometry; LVEF, left ventricle ejection fraction; and LVFS, left ventricular fractional shortening.

its efficacy in mitigating ferroptosis-mediated cardiac injury in ALDH2*2 mice.

Furthermore, Fer-1 pretreatment on day 3 after MI eliminated the increased serum LDH activity levels (Figure 2G) and infarct tissue Fe^{2+} (a ferroptosis marker) levels in ALDH2*2 mice compared with WT mice (Figure 2H). Additionally, bioactive lipid AA was also significantly elevated in the serum of ALDH2*2 mice after MI, which was attenuated by Fer-1 pretreatment (Figure 2I). In contrast, 15d-PGD_2, the 14,15-DHET/14,15-epoxy eicosatetraenoic acid ratio, and ALOX15 enzymatic products (13-HODE and 15-HETE) trended higher in vehicle-treated ALDH2*2 compared with WT mice after MI but did not reach statistical significance after false discovery rate correction, and levels also remained comparable in Fer-1–treated groups (Figure 2I). All of these data revealed that inhibiting ferroptosis at the AMI stage confers cardioprotection in ALDH2*2 mice. Given that Alda-1 (an ALDH2 agonist) and Necrostatin-1 (Nec-1; a necroptosis inhibitor) reduce heart injury after I/R,[34,35] we also pretreated mice with vehicle, Nec-1, or Alda-1 (Figure S3G). In the acute ischemic model, Nec-1 significantly reduced LDH activity levels only in ALDH2*2 mice, whereas Alda-1 showed no significant effect (Figure S3H). Because Nec-1 can inhibit both necroptosis and ferroptosis,[36] these findings suggest that targeting ferroptosis effectively mitigates ischemic cardiac injury in ALDH2*2 mice after MI.

Taken together, the ALDH2*2 mutant exacerbates AHF by promoting ferroptosis after MI, an effect significantly mitigated by Fer-1 pretreatment.

ALDH2*2 Mutation Exacerbates Ferroptosis in Ischemic Heart Injury With Upregulated Ferroptosis Marker Proteins

HIF-1α (hypoxia-inducible factor 1-alpha) protein levels were upregulated after ischemic injury, as reported previously,[37] but significantly attenuated in ALDH2*2 mice after MI (Figure 3A and 3B). Concurrently, ALDH2 protein levels were significantly reduced in WT mice after MI (Figure 3A and 3C), consistent with known ALDH2 downregulation in MI.[38] ALDH2 levels were further diminished in ALDH2*2 mice (Figure 3A and 3C), which aligns with the dominant-negative effect of the ALDH2*2 mutation on protein stability.[23] These findings suggest that the ALDH2*2 mutation may promote ferroptosis and worsen heart injury by reducing cardioprotective ALDH2 protein levels.

We then performed targeted lipidomic analysis on cardiac infarct tissues to identify ferroptosis-related lipid peroxide species altered in ALDH2*2 mice on day 3 after MI. WT infarct tissues only showed markedly increased oxygenated phospholipids compared with WT sham controls (Figure 3D). ALDH2*2 infarct tissues demonstrated increased levels of phosphatidylcholine and PE species, including both nonoxygenated and oxygenated fatty acids (Figure 3D). We noticed basic nonoxygenated fatty acids, including peroxidation-prone phospholipids (AA [AA-PE/phosphatidylcholine, C20:4] and AdA [AdA-PE/phosphatidylcholine, C22:4]), increased specifically in ALDH2*2 infarct tissues. These findings suggest enhanced PUFA-CoA synthesis (providing substrates for the COX, LOX, and cytochrome P450 monooxygenase pathways),[39] consistent with ferroptosis activation. Given that ferroptosis relies on iron-dependent lipid peroxidation, and the heart is an organ with high iron metabolism, we assessed key proteins in these processes. We measured ACSL4, a critical driver of PUFA-phospholipid (PL) metabolism and ferroptosis sensitivity, and TFRC, a key iron metabolism protein,[9] in infarct tissues on day 3 after MI and sham left ventricular tissues. Protein and mRNA levels of both TFRC and ACSL4 were upregulated in WT infarct tissues after MI compared with sham controls (Figure 3E through 3G). ALDH2*2 infarct tissues showed further increases in TFRC and ACSL4 protein levels (Figure 3E and 3F) without changes in mRNA levels compared with WT infarct tissues (Figure 3G), indicating post-transcriptional regulation. Moreover, significantly elevated TFRC expression in infarct regions was further confirmed by immunohistochemical analysis in ALDH2*2 compared with WT mice on day 3 after MI (Figure S4A and S4B). Consistent with increased iron transport, ICP-mass spectrometry revealed elevated total iron content in ALDH2*2 infarct tissues (Figure S4C), accompanied by increased serum transferrin levels in ALDH2*2 mice compared with WT mice on day 3 after MI (Figure S4D). These findings support upregulated iron metabolism in ALDH2*2 mice after MI. We also examined autophagy-related iron release mechanisms in infarct tissues.[40] The expressions of FTH (ferritin heavy chain), predominantly expressed in cardiomyocytes than ferritin light chain[41] and NCOA4 (nuclear receptor coactivator 4; a key cargo receptor in ferritinophagy) did not show any significant change between WT and ALDH2*2 mice after MI (Figure S4E and S4F). However, HMOX1 (heme oxygenase 1) was markedly elevated in ALDH2*2 mice (Figure S4E and S4F). These findings implicate TFRC-mediated iron

ORIGINAL RESEARCH ARTICLE

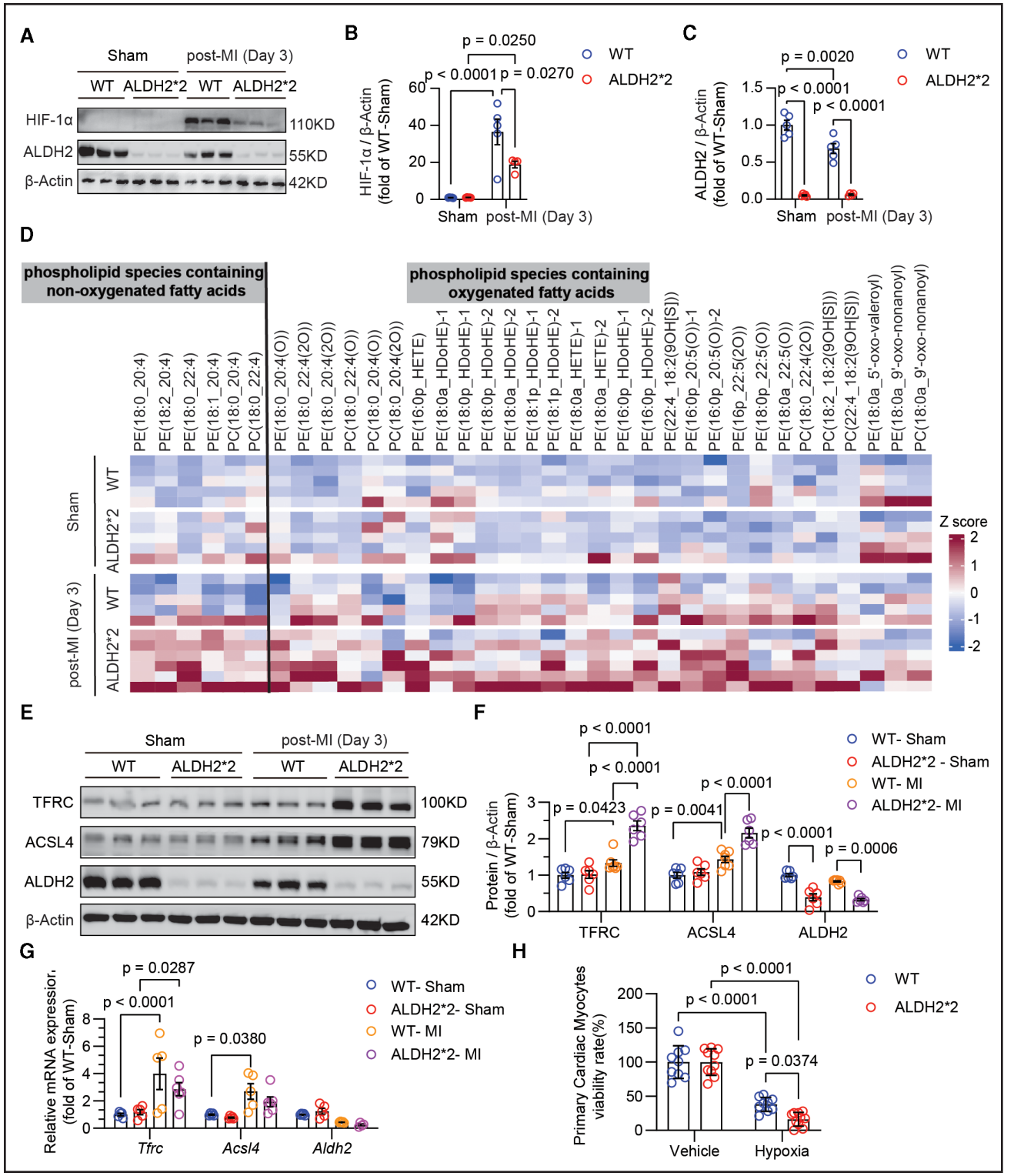

Figure 3. Oxidized phospholipids and the ferroptosis-related proteins TFRC and ACSL4 increased specifically in the infarct tissues of ALDH2*2 mice.

A, Representative immunoblot images of HIF-1α (hypoxia-inducible factor 1-alpha), ALDH2 (acetaldehyde dehydrogenase 2), and β-actin in the infarct tissues from wild-type (WT) and ALDH2*2 mice on day 3 after MI or sham surgery (n=3 per group). **B** and **C**, Quantification of the immunoblot results from **A** (n=5, 5, 5, and 4 per group). **D**, Targeted metabolomics analysis of oxidized phospholipids, including both nonoxygenated and oxygenated fatty acids, in the infarct tissues (WT-sham, ALDH2*2-sham, WT-myocardial infarction [MI], and ALDH2*2-MI; n=5, 5, 5, and 6 for each group, respectively). Upregulation, red; downregulation, blue. The color scale represents the *Z* score. **E**, Representative immunoblot images of the ferroptosis marker proteins TFRC (transferrin receptor) and ACSL4 (acyl-coenzyme A synthetase long-chain family member 4) alongside ALDH2 and β-actin in infarct tissues on day 3 after MI or sham surgery (n=3 per group). (*Continued*)

Figure 3 Continued. **F**, Quantitation of protein levels from **E** (WT-sham, ALDH2*2-sham, WT-MI, ALDH2*2-MI; n=6, 6, 7, and 6 per group, respectively). **G**, RT-PCR analysis of *Tfrc*, *Acsl4*, and *Al*dh2 mRNA in myocardial infarct tissues collected on day 3 after MI. Expression was normalized to β-actin and presented as fold change relative to WT-sham controls (WT-sham, ALDH2*2-sham, WT-MI, ALDH2*2-MI; n=5, 5, 5, and 6 per group, respectively). Data points represent biological replicates with 3 technical replicates per sample. **H**, Cell viability of WT and ALDH2*2 primary cardiomyocytes after 48 hours of treatment with hypoxia or vehicle (WT-vehicle, ALDH2*2-vehicle, WT-hypoxia, ALDH2*2-hypoxia, n=9, 10, 9, and 10 for each group). Data are presented as mean±SEM in **B**, **C**, **F**, and **G** and as mean±SD in **H**. Statistical analysis was performed using 2-way ANOVA (**B** and **C** and **F** through **H**). RT-PCR indicates real-time quantitative polymerase chain reaction.

uptake and HMOX1-driven ferrous ion release as the dominant iron sources over ferritinophagy, contributing to ferroptosis in ALDH2*2 hearts after MI.[42]

We also detected key antioxidative proteins linked to ferroptosis. Both DHODH (dihydroorotate dehydrogenase), FSP1, and GPX4 (glutathione peroxidase 4) protein levels were significantly downregulated in both WT and ALDH2*2 infarct myocardium compared with their respective sham controls. In contrast, these protein levels showed no significant differences between WT and ALDH2*2 genotypes (Figure S4G and S4H). Meanwhile, dihydrofolate reductase was significantly increased after MI compared with sham controls, whereas GCH1 (GTP cyclohydroxylase 1) levels remained comparable between WT and ALDH2*2 genotypes (Figure S4G and S4H). These findings suggest a broad attenuation of ferroptosis defense mechanisms after MI, particularly mitochondrial DHODH and CoQ10-dependent systems (GPX4 and FSP1), regardless of ALDH2 genotype. As the atrium and brain regions were prone to ischemia and influenced by the ALDH2*2 mutation,[43] we also examined TFRC, ACSL4, GPX4, and ALDH2 in these tissues. In atrium tissues, ALDH2 levels were markedly downregulated in ALDH2*2 mice compared with WT mice on day 3 after MI, with no changes in TFRC, ACSL4, or GPX4 protein levels (Figure S5A and S5B). In the brain tissues, ACSL4 levels were markedly elevated in ALDH2*2 sham groups compared with WT controls and further increased after MI, whereas TFRC and GPX4 levels remained unchanged between ALDH2*2 and the WT (Figure S5C and S5D). These findings indicate that TFRC and ACSL4 protein levels were specifically upregulated in ALDH2*2 heart infarct tissues compared with WT infarct tissues, highlighting their potential role in exacerbating ferroptosis and injury after MI.

Primary cardiomyocytes isolated from WT and ALDH2*2 mice were exposed to $CoCl_2$ to induce hypoxia, simulating ischemic injury in vitro. ALDH2*2 myocytes showed greater susceptibility to hypoxia-induced cell death (Figure 3H), accompanied by elevated oxidized phospholipids (Figure S6A). Hypoxia-induced cell death could be mitigated by cotreatment with the ferroptosis inhibitor Fer-1, the iron chelator DFO (deferoxamine), the necroptosis inhibitor Nec-1, or the apoptosis inhibitor benzyloxycarbonyl-Val-Ala-Asp-fluoromethylketone (Z-VAD-FMK; Figure S6B). In contrast, autophagy inhibition via 3-methyladenine (3-MA) provided only partial protection (Figure S6C). Nec-1 has been reported to suppress both necroptosis and ferroptosis during heart I/R injury.[34] Numerous pathways involved in apoptosis,[44] necroptosis,[45] and autophagy[46] contribute to ALDH2 deficiency–induced cardiac I/R injury.[15] Collectively, these findings suggest that targeting ferroptosis, potentially alongside other regulated cell death pathways, can be a novel therapeutic approach for protecting ALDH2*2 primary cardiomyocytes under hypoxia conditions.

Taken together, the ALDH2*2 mutation exacerbates ischemic heart injury by promoting cardiomyocyte ferroptosis, which is associated with upregulated TFRC and ACSL4 protein levels in infarct tissues despite unchanged mRNA levels.

ALDH2 Deficiency Renders Cardiomyocytes Susceptible to Ferroptosis by Promoting *Tfrc* and *Acsl4* mRNA Translation

In primary cardiac myocytes of the WT, hypoxia induced increased protein levels of HIF-1α, TFRC, and ASCL4 and decreased ALDH2 (Figure S6D through S6G). In ALDH2*2 cells, TFRC and ASCL4 levels were further elevated under hypoxia, with ALDH2 further decreased and no significant change in HIF-1α compared with hypoxia-treated WT cells (Figure S6D through S6G). These results suggest that the ALDH2*2 variant exacerbates hypoxia-driven ferroptosis in cardiomyocytes, whereas the HIF-1α response remains unaffected.

To dissect the roles of protein synthesis or degradation in affecting these protein levels, we treated cardiomyocytes with the protein synthesis inhibitor cycloheximide. Under hypoxia conditions, ALDH2*2 cells showed elevated TFRC and ACSL4 levels compared with the WT, but these differences were abolished after 6 hours of cycloheximide treatment, whereas ALDH2 remained downregulated (Figure S6H through S6K). These results suggest that protein synthesis pathways play a more important role than degradation in the upregulation of TFRC and ACSL4 in ALDH2*2 cells under hypoxia conditions.

We also treated the human cardiomyocyte cell line AC16 with RSL3 to induce ferroptosis and found that ALDH2-deficient cells (shA, Aldh2 KD) were more sensitive to ferroptosis compared with the control (shNC) (IC_{50}: shNC, 1.69 μM; sh *Aldh2*, 0.11 μM) (Figure 4A). To verify translational regulation, polysome profiling was performed on AC16 cells under both vehicle (Figure S7A) and RSL3 treatment conditions (Figure S7B). Under vehicle conditions, ALDH2-deficient cells showed decreased mRNA in free to light polysome (LP)

ORIGINAL RESEARCH ARTICLE

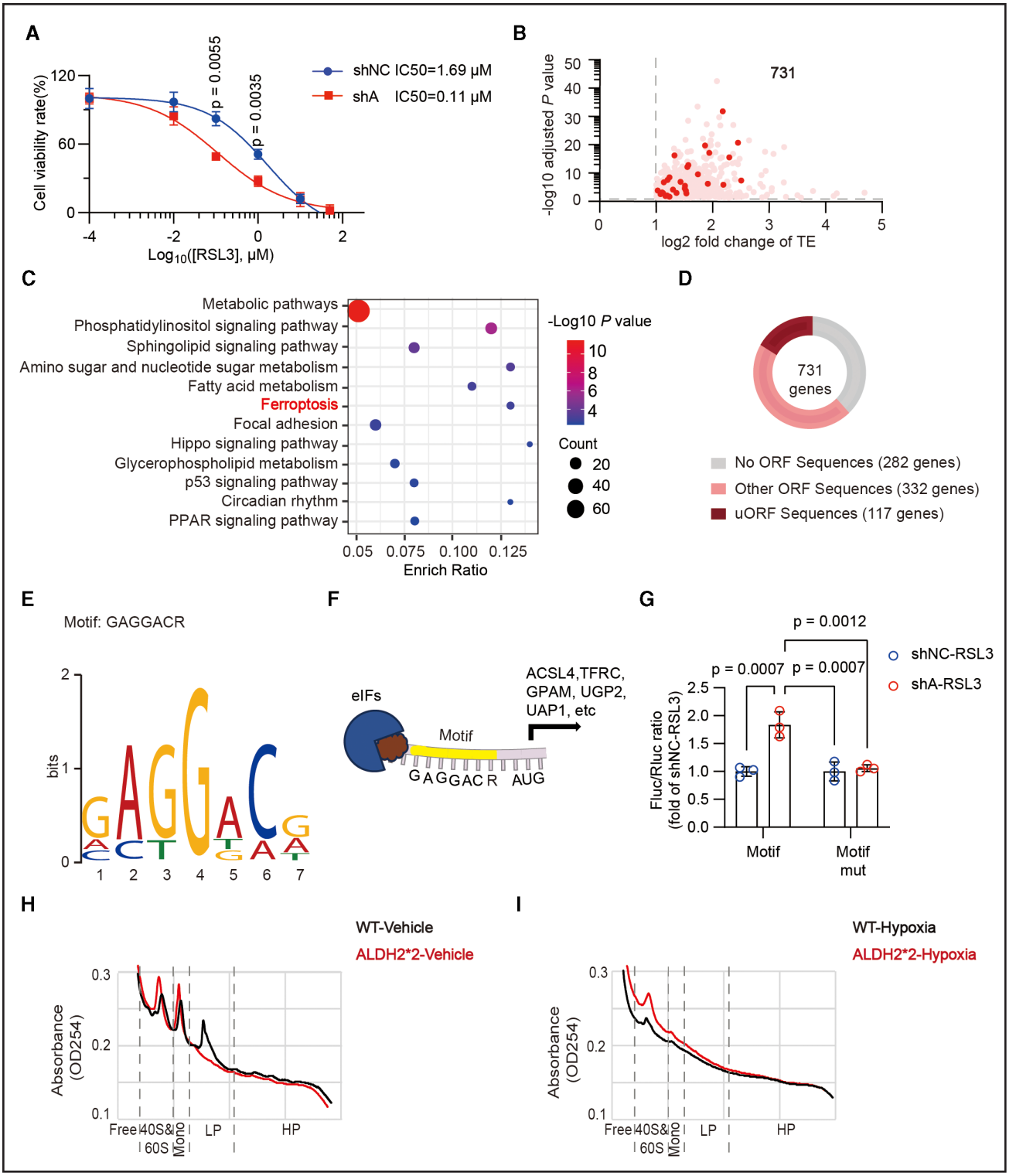

Figure 4. ALDH2 deficiency promotes cardiomyocyte ferroptosis and upregulates translation of selectively mRNA.
A, Cell viability of AC16 shNC (negative control, PLKO.1-Puro empty vector) and shA (Aldh2 knockdown) cells after 12 hours of treatment with various concentrations of RSL3 to induce ferroptosis (n=5 per concentration). **B**, Translation efficiency (TE) profiling with ferroptosis treatment (1 μM RSL3, 12 hours). Volcano plot identifies 731 transcripts with significantly elevated translation efficiency in shA vs shNC cells (fold change>2, adjusted *P*<0.05). For the complete data set, see Table S5 (731 transcripts; n=2 per group). Red dots specifically highlight 29 genes that were annotated as ferroptosis related in the FerrDb database. **C**, Kyoto Encyclopedia of Genes and Genomes pathway enrichment analysis. "Count" denotes the number of differentially expressed transcripts (from **B**) mapped to each pathway. *x* axis: enrich ratio = (differentially expressed transcripts in pathway)/(total annotated transcripts in pathway). **D**, Pie chart depicting the classification of the 731 transcripts from **B**; 449 contain defined open reading frames (ORFs), with 117 of those having upstream ORFs strictly localized to the 5′ untranslated region. (*Continued*)

Figure 4 Continued. The remaining 332 genes have ORFs located downstream or span both upstream ORFs and coding regions (eg, coding sequence, truncORF, or dORF). **E**, MEME Suite analysis identified the conserved GAGGACR motif among the 117 upstream ORFs from **D**. **F**, Schematic of the GAGGACR motif in 5′ untranslated regions that included key genes (ACSL4, TFRC GPAM, UGP2, and UAP1) from top-enriched pathways from **C**. **G**, Luciferase reporter assays comparing wild-type (WT) GAGGACR with mutant motifs (Motif mut, CACCACC) in the 5′ untranslated region, performed in shNC and shA AC16 cells under ferroptosis conditions (1 μM RSL3, 12 hours, n=3 per group). **H** and **I**, Polysome profiles of WT and ALDH2*2 primary cardiomyocytes that were treated with vehicle control (**H**) and hypoxia (**I**). Isolated ribosomal fractions include free ribosomes, 40S and 60S subunits, monosomes, light polysomes (LPs), and heavy polysomes (HPs). Data are presented as mean±SD, with statistical analysis performed using 2-way ANOVA (**A** and **G**). eIF indicates eukaryotic initiation factor; GPAM, glycerol-3-phosphate acyltransferase, mitochondrial; Ribo-seq, ribosome profiling; UAP1, UDP-N-acetylglucosamine pyrophosphorylase 1; and UGP2, UDP-glucose pyrophosphorylase 2.

fractions without significant change in heavy polysome (HP) fractions, indicating upregulated translation (Figure S7A). Under ferroptosis conditions, control cells showed downregulated translation, whereas ALDH2-deficient cells further exacerbated this suppression of translation in that HP fractions were slightly decreased (Figure S7B). Quantitative polymerase chain reaction (qPCR) analysis of polysome mRNA distribution revealed that *Gapdh* (positive control) was more efficiently translated in ALDH2-deficient cells under vehicle conditions, as evidenced by its redistribution from the free and LP fractions to HP fractions (Figure S7C). Still, no changes were observed under ferroptosis conditions (Figure S7D), likely because of RSL3-induced ROS inhibiting translation.[47] The noncoding RNA *hY1* (negative control) also showed no differences between ALDH2-deficient and control cells, whether under vehicle (Figure S7E) or ferroptosis conditions (Figure S7F).

Notably, in ALDH2-deficient cells under vehicle treatment, the translation of *Tfrc* was slightly suppressed. This was characterized by an increased mRNA abundance in the free to LP fractions and a concomitant decrease in HP fractions (Figure S7G). Conversely, under ferroptosis conditions, *Tfrc* translation was significantly promoted in ALDH2-deficient cells, as evidenced by a decrease in its mRNA abundance in the free to LP fractions and a concurrent increase in HP fractions (Figure S7H). Similarly, *Acsl4* translation showed no significant change under vehicle treatment (Figure S7I) but was significantly promoted under ferroptosis conditions in ALDH2-deficient cells, with a clear shift of mRNA abundance toward HP fractions (Figure S7J). These findings confirmed that ALDH2 deficiency promotes the active translation of *Tfrc* and *Acsl4* under ferroptosis conditions.

In summary, ALDH2 deficiency increases cardiomyocyte susceptibility to ferroptosis with upregulated translation of the ferroptosis marker proteins TFRC and ACSL4.

Genome-Wide Translation Regulation in ALDH2-Deficient Cells Under Ferroptosis Conditions

To identify genes affected by ALDH2 deficiency under ferroptosis, we performed Ribo-seq to capture ribosome-bound mRNA fragments. Translation efficiency (TE) for each transcript was calculated as the log2-transformed ratio of Ribo-seq Fragments Per Kilobase of transcript per Million mapped fragments (FPKM) to RNA-sequencing FPKM, revealing distinct patterns of translational regulation. Under ferroptosis conditions, sh*Aldh2* AC16 cells exhibited elevated TE versus shNC cells, with 731 transcripts showing significant TE upregulation (fold change>2, adjusted $P<0.05$) and 473 transcripts displaying downregulation (Figure 4B; Table S5). Among the 731 transcripts, 29 genes were annotated as ferroptosis related in the FerrDb database (Figure 4B; Table S5). Kyoto Encyclopedia of Genes and Genomes pathway analysis of genes with upregulated TE revealed enrichment in metabolic pathways, fatty acid metabolism, and ferroptosis (Figure 4C; Table S5). Among the 731 genes, 449 harbored precisely annotated open reading frames (ORFs), with 117 upstream ORFs exclusively localized to 5′ untranslated regions (UTRs) (Figure 4D). A conserved motif, GAGGACR (R: A/G; E value: 5.42e−003) (Figure 4E), was significantly enriched in 46% (54/117) of upstream ORF–containing transcripts, including ferroptosis-related genes (ACSL4 and TFRC), metabolic genes (GPAM, UGP2, and UAP1), and genes from other less prominent pathways (Figure 4F; Table S5). Luciferase reporters with WT GAGGACR motifs in their 5′ UTRs showed enhanced translation in ALDH2-deficient cells under ferroptosis, whereas mutated motifs (G to C) abolished this effect (Figure 4G). Mutating the GAGGACR motif (G to C) in the 5′ UTRs of TFRC (mut x 1: one motif mutated; mut x 2, both motifs mutated) and ACSL4 (Figure S8A) as well as GPAM, UGP2, and UAP1 (mut x 1; mut x 2) (Figure S8B) suppressed their ferroptosis-associated translational induction. These findings implicate the GAGGACR motif as a critical regulatory element driving the translation of ferroptosis and metabolism-related genes in ALDH2-deficient cells.

We extended our analysis to assess translation in primary cardiomyocytes. Under vehicle conditions, ALDH2-deficient cells showed a decrease in mRNA abundance in the free to LP fractions, a profile consistent with upregulated translational activity (Figure 4H). Hypoxia further suppressed translation in WT myocytes, as evidenced by decreased polysome absorbance across all fractions (Figure 4I) compared with WT normal cells (Figure 4H), consistent with hypoxia-induced, ROS-mediated translation inhibition.[47] ALDH2*2 myocytes showed further translation suppression, with increased polysome absorbance in free to LP fractions and no change in HP fractions compared with WT cells under

hypoxia (Figure 4I). ALDH2*2 myocytes under hypoxia showed severe translation suppression (Figure 4I) compared with AC16 cells undergoing RSL3-induced ferroptosis (Figure S7B), suggesting heightened ROS stress in hypoxia-treated cardiomyocytes. Notably, qPCR analysis revealed that β-*actin* (positive control) mRNA distribution was unchanged in ALDH2*2 and WT cells under both vehicle and hypoxia treatment (Figure S9A and S9B). *Tfrc* translation showed no changes under vehicle conditions (Figure S9C), but mRNA abundance significantly increased in ALDH2*2 myocytes under hypoxia treatment compared with WT cells (Figure S9D). Similar changes were observed in *Acsl4* under vehicle (Figure S9E) and hypoxia conditions (Figure S9F), confirming hypoxia-induced translational upregulation. *Uap1* translation also showed no change under vehicle conditions (Figure S9G) but was significantly upregulated in ALDH2*2 myocytes under hypoxia conditions (Figure S9H). In contrast, *Gpat4*, a ferroptosis-related gene lacking the GAGGACR motif in its 5′ UTR, showed no translational change under vehicle (Figure S9I) or hypoxia (Figure S9J) conditions. These findings suggested that genes with the GAGGACR motif were primarily activated at the translational level in response to hypoxic stress.

Together, these data indicate that hypoxic ALDH2*2 cardiomyocytes experience global translational repression while selectively enhancing translation of GAGGACR motif–containing transcripts, especially the ferroptosis-related genes *Tfrc* and *Acsl4*. This targeted translation amplifies redox imbalance and lipid peroxidation, which, in turn, further suppresses bulk protein synthesis.

eIF3E Regulates GAGGACR Motif–Dependent Translation in ALDH2-Deficient Cardiomyocytes

We propose that ALDH2 modulates the TE of genes with the GAGGACR motif by influencing specific components of the translation machinery. Central to this process is eIF4G, a scaffolding protein that bridges the eIF3 complex, the eIF4E/cap-mRNA complex, and ribosomes during cap-dependent translation.[48] Notably, eIF3E, a noncore subunit of eIF3,[49] interacts directly with eIF4G1 (a member of the eIF4G protein family) to regulate the translation of specific mRNAs, including those critical for mitochondrial function and skeletal muscle health, with *Tfrc* and *Acsl4* among the regulated genes.[50,51] Additionally, eIF4G1 contains binding sites for both eIF3E and mRNA,[52,53] positioning it as a potential mediator of the effects of ALDH2.

We further hypothesize that ALDH2 enhances eIF3E-eIF4G1 interaction, thereby selectively modulating the TE of genes harboring the GAGGACR motif. In ALDH2*2 primary cardiomyocytes under hypoxic conditions, levels of the noncore subunit eIF3E, the core subunit eIF3G, the core scaffolding component eIF4G1, phosphorylated eIF4E, and total eIF4E remained unchanged compared with WT myocytes despite reduced ALDH2 protein levels (Figure 5A and 5B). Strikingly, coimmunoprecipitation assays confirmed enhanced eIF3E-eIF4G1 binding without affecting the binding levels of eIF3G (the core factor of the eIF3 complex) in ALDH2*2 primary cardiomyocytes compared with WT myocytes under hypoxia (Figure 5A and 5C). These results suggest that ALDH2 deficiency enhances eIF3E (within the eIF3 complex)-eIF4G1 interaction, providing a mechanistic basis for preferential translation of GAGGACR motif–bearing genes (eg, *Tfrc* and *Acsl4*), despite global translation suppression.

To determine whether eIF3E-eIF4G1 interaction regulates the translation of GAGGACR motif–containing genes in ALDH2-deficient cells during ferroptosis, we employed luciferase reporter assays on cells transfected with constructs including the GAGGACR motifs (WT or mutated) in 5′ UTRs, along with ATP5H (an eIF3E-regulated positive control) and PSMB6 (negative control).[54] ALDH2 KD increased luciferase activity for the GAGGACR WT motif and ATP5H under ferroptosis conditions (Figure 5D). Conversely, eIF3E KD abolished this induction (Figure 5D and 5E), whereas motif-mutant and PSMB6 remained unaffected (Figure 5D and 5E), confirming eIF3E's specificity for GAGGACR-dependent translation. RNA immunoprecipitation (RNA-IP) assays further revealed that *Tfrc* and *Acsl4* mRNAs showed enhanced binding to eIF3E in ALDH2-deficient cells compared with controls during ferroptosis, whereas *Dst* (positive control),[54] and *Gapdh* (negative control) remained unchanged (Figure 5F). To exclude potential indirect effects from other factors of eIF3, we performed eIF3K KD as a negative control. Because eIF3K depletion minimally disrupts the eIF3 complex but retains the eIF3A to eIF3J subunits and eIF3E binding, it is ideal for isolating eIF3E-specific effects.[49] In sg *Aldh2* cells under ferroptosis, eIF3K KD did not affect GAGGACR motif–dependent translation (Figures S10A and S10B). These results confirm that eIF3E specifically regulates the translation of GAGGACR motif–containing mRNAs through its binding to eIF4G1.

These findings demonstrate that eIF3E selectively regulates the translation of GAGGACR motif–containing genes (including *Tfrc* and *Acsl4*) in ALDH2-deficient cells under ferroptosis, driving ferroptosis progression.

ALDH2 Competitively Binds eIF3E to Modulate Translation

eIF3E protein levels decreased significantly in infarct tissues on day 3 after MI compared with sham left ventricular tissues (Figure S10C and S10D), likely because of hypoxia-induced ROS-mediated translation inhibition.[47] No differences were observed between WT and ALDH2*2 mice, whether in sham or MI groups

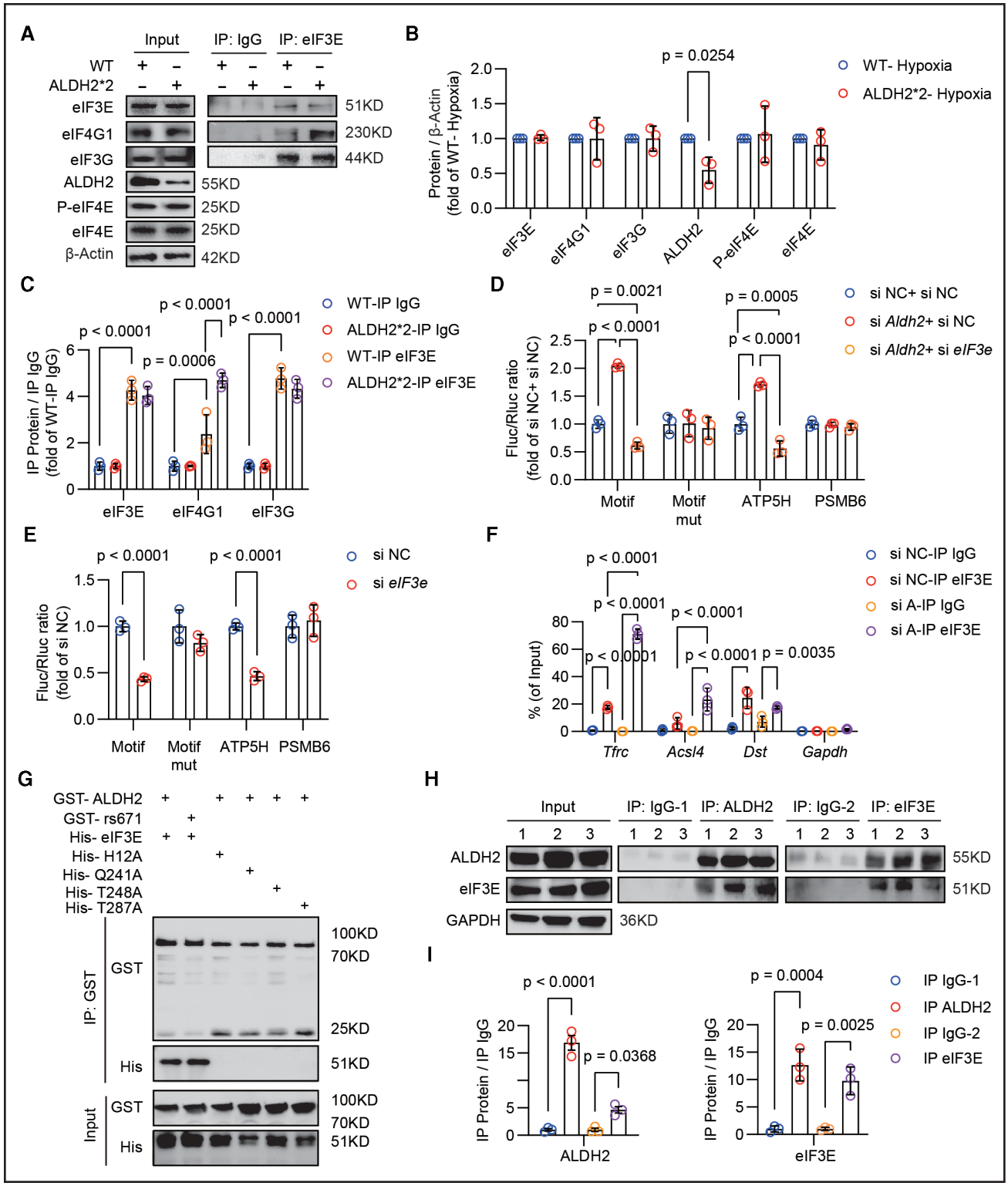

Figure 5. eIF3E regulates the translation of GAGGACR motif-containing genes, including *Tfrc* and *Acsl4*, promoting ferroptosis in ALDH2-deficient cells.

A, Representative immunoblotting images from a coimmunoprecipitation assay using anti-IgG and anti-eIF3E antibodies. **B**, Quantification of input protein levels from **A** (n=3 per group). **C**, Quantification of coimmunoprecipitation protein levels from **A** (n=3 for each group). **D**, Luciferase activity in AC16 cells subjected to ferroptosis (1 μM RSL3, 12 hours, n=3 per group) with the following treatments: si negative control (NC) + si NC, si *Aldh2* + si NC, and si *Aldh2* + si *eIF3e*. **E**, Luciferase activity in untreated (normal) AC16 cells (n=3 per group), transfected with Motif (identified in Figure 4E: GAGGACR), Motif mut (G to C: CACCACC), ATP5H (positive eIF3E-regulated control), and PSMB6 (negative control). Same reporters as in **D**. **F**, RNA immunoprecipitation assay in AC16 cells with ferroptosis treatment (1 μM RSL3, 12 hours, n=3 per group) using anti-IgG and anti-eIF3E antibodies. **G**, Glutathione S-transferase pull-down assay using recombinant His-tagged eIF3E WT (*Continued*)

Figure 5 Continued. and mutants His-tagged eIF3E (H12A, Q241A, T248A, T287A) incubated with glutathione S-transferase–tagged ALDH2 (acetaldehyde dehydrogenase 2) or glutathione S-transferase–tagged ALDH2 rs671 mutant proteins. **H**, Coimmunoprecipitation assay in left ventricular tissues from 3 heart failure patients (all carriers are ALDH2*2 variant; n=3). Lanes 1, 2, and 3 correspond to the individual patients listed in Table S1. **I**, Quantitation of IP protein levels from **H**. Results are presented as mean±SD. Statistical analysis was performed using a 2-tailed Student *t* test (**B** and **E**), 1-way ANOVA (**D**), and 2-way ANOVA (**C**, **F**, and **I**). ATP5H indicates ATP synthase, H^+ transporting, mitochondrial F_0 complex, subunit d; co-IP, coimmunoprecipitation; Dst, dystonin; eIF3E, eukaryotic initiation factor 3 E; eIF3G, eukaryotic translation initiation factor 3 subunit G; eIF4E, eukaryotic translation initiation factor 4 subunit E; eIF4G1, eukaryotic translation initiation factor 4 gamma 1; P-eIF4E, phospho-eIF4E; GST, glutathione S-transferase; IgG, immunoglobulin G; and PSMB6, proteasome 20S subunit beta 6.

(Figure S10C and S10D). Gromacs modeling predicted a potential protein interaction between ALDH2 and eIF3E (Figure S10E). The predicted ALDH2 interaction sites on eIF3E (A9, H12, Q241, T248, and T287) reside within its N-terminal two-thirds (Figure S10E), a region critical for eIF4G1 binding.[52] The interaction sites do not overlap with the ALDH2*2 mutant sites (E504K). We successfully purified 4 point mutant proteins of eIF3E: H12A, Q241A, T248A, and T287A (Figure 5G). We found that all 4 mutants abolished the interaction between eIF3E and ALDH2 (Figure 5G), suggesting that ALDH2 competes with eIF4G1 for binding at these sites. Interestingly, the ALDH2 rs671 mutant retained eIF3E binding comparable with WT ALDH2 (Figure 5G), consistent with computational predictions.

To experimentally validate the interaction, we performed coimmunoprecipitation experiments using the left ventricular tissues from 3 heart transplant patients with heart failure (Table S1). We found that ALDH2 and eIF3E were pulled down with each other (Figure 5H and 5I). Consistent findings were observed in the left ventricular tissues of WT mice, and less eIF3E was pulled down in ALDH2*2 mice, correlating with reduced ALDH2 levels (Figure S10F and S10G). Additionally, subcellular fractionation of WT cardiomyocytes revealed that eIF3E predominantly localizes to the cytosol, as indicated by the localization of VDAC (a mitochondrial marker) and GAPDH (a cytosolic marker) (Figure S11A and S11B), supporting cytoplasmic ALDH2-eIF3E interaction.

Together, these results suggested that ALDH2 competitively binds to the N-terminal two-thirds of eIF3E, a region critical for eIF4G1 interaction, thereby modulating translation. This mechanism is conserved across species and validated in both human and murine models.

ALDH2 Regulates Ferroptosis via eIF3E Interaction

To provide further evidence that ALDH2/eIF3E interaction is essential for regulating ferroptosis, we conducted ALDH2 KD, ALDH2 rs671/ALDH2 WT overexpression, and eIF3E KD experiments in AC16 cells under RSL3-induced ferroptosis. ALDH2 rs671 or ALDH2 WT overexpression restored cell survival in ALDH2-deficient cells (Figure S12A) and reduced TFRC and ACSL4 protein levels without altering eIF3E levels (Figure S12B and S12C). *Tfrc* and *Acsl4* mRNA levels remained unchanged (Figure S12D), indicating translation rather than transcription regulation.

Similarly, eIF3E KD in ALDH2-deficient AC16 cells rescued cell survival (Figure S12E), reduced TFRC and ACSL4 protein levels (Figure S12F and S12G), and left *Tfrc* and *Acsl4* mRNA levels unaffected (Figure S12H), confirming ALDH2's regulation of ferroptosis through eIF3E. Furthermore, multiple oxidized phospholipids identified in hypoxic ALDH2*2 cardiomyocytes, were significantly increased during RSL3-induced ferroptosis compared with vehicle or H_2O_2-induced cell necrosis (Figure S13A). These increases were further exacerbated in ALDH2-deficient cells but mitigated by ALDH2 rs671/ALDH2 WT overexpression (Figure S13B). Overexpression of ALDH2 WT or rs671 or silencing eIF3E reduced lipid peroxidation (Figure S13C and S13D).

In conclusion, these findings suggest that ALDH2 modulates ferroptosis by physically interacting with eIF3E (within the eIF3 complex). Under ferroptosis or hypoxic stress, ALDH2 deficiency promotes eIF3E-eIF4G1 binding, enhancing the translation of ferroptosis-related mRNAs, such as *Tfrc* and *Acsl4*, to drive ferroptosis.

Cardiomyocyte-Specific KD of EIF3E Improves ALDH2*2 Heart Function by Decreasing Ferroptosis in MI

To further verify that ALDH2*2 aggravates cardiomyocyte ferroptosis through eIF3E during MI, we employed a MI mouse model with cardiomyocyte-specific eIF3E KD (Figure 6A). In ALDH2*2 mice, eIF3E KD significantly enhanced cardiac function versus AAV (adeno-associated virus)-control, evidenced by elevated LVEF (Figure 6B) and LVFS (Figure 6C) and reduced left ventricular internal diameter versus WT eIF3E KD (Figure S14A) without altering interventricular septum thickness at end-diastole (IVSd) (Figure S14B). Additionally, cardiomyocyte-specific eIF3E KD significantly decreased the scar area in ALDH2*2 mice but not in WT mice 28 days after MI (Figure 6D and 6E; Table S4-3). Importantly, cardiomyocyte-specific eIF3E KD did not lead to cardiomegaly nor myocardial hypertrophy after MI, as indicated by the unaltered wheat germ agglutinin and Ki67 (cell proliferation) staining in all groups 28 days after MI (Figure S14C through S14F; Table S4-4 and S4-5). These results suggest that ALDH2*2 exacerbates cardiac ischemic injury via eIF3E-mediated ferroptosis.

On day 3 after MI, eIF3E KD in ALDH2*2 mice significantly reduced serum LDH activity levels (Figure 6F), oxidized phospholipids in infarct tissues (Figure 6G), and

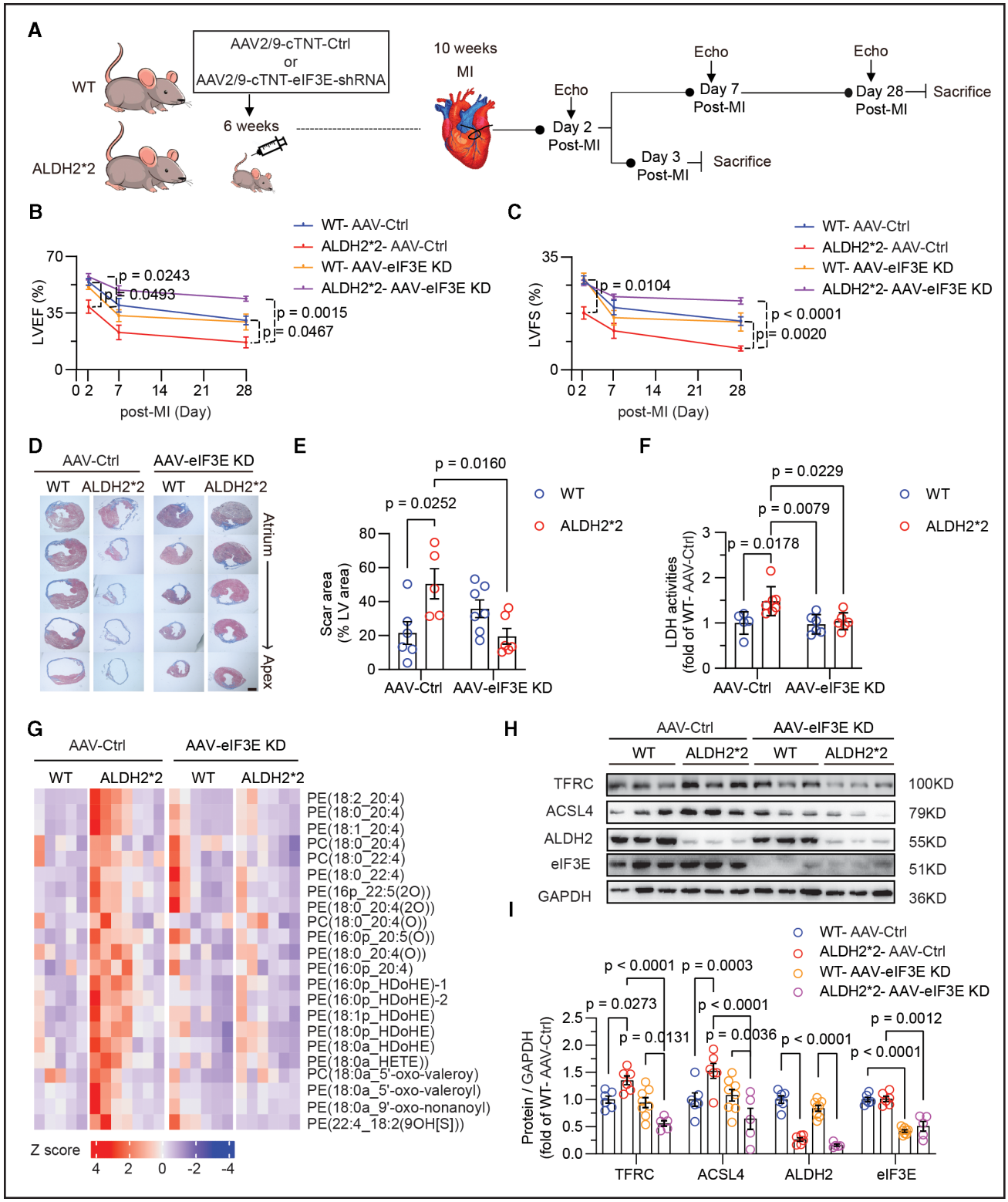

Figure 6. Cardiomyocyte-specific knockdown of eIF3E improves ALDH2*2 heart function by mitigating ferroptosis.
A, Schematic depicting the experimental strategy. Six-week-old mice were administered either AAV2/9-cTNT-control (Ctrl) or AAV2/9-cTNT-eIF3E-shRNA (eIF3E KD) virus via tail vein injection. **B** and **C**, LVEF and LVFS were assessed in mice (WT- AAV-Ctrl, ALDH2*2- AAV-Ctrl, WT- AAV-eIF3E KD, and ALDH2*2- AAV-eIF3E KD; n=6, 5, 7, and 6, respectively). Statistical testing used 2-way ANOVA with modification for multiple comparisons. **B**, On day 2 after MI, ALDH2*2- AAV-Ctrl vs WT- AAV-Ctrl *P*=0.0493, ALDH2*2- AAV-eIF3E KD vs ALDH2*2- AAV-Ctrl *P*=0.0243; on day 28 after MI, ALDH2*2- AAV-Ctrl vs WT- AAV-Ctrl *P*=0.0467, ALDH2*2- AAV-eIF3E KD vs ALDH2*2- AAV-Ctrl *P*=0.0015. **C**, On day 2 after MI, ALDH2*2- AAV-Ctrl vs WT- AAV-Ctrl *P*=0.0104, ALDH2*2- AAV-eIF3E KD vs ALDH2*2- AAV-Ctrl *P*=0.0193; on day 28 after MI, ALDH2*2- AAV-Ctrl vs WT- AAV-Ctrl *P*=0.0020, ALDH2*2- AAV-eIF3E KD vs ALDH2*2- AAV-Ctrl *P*<0.0001. (*Continued*)

Figure 6 Continued. **D**, Representative Masson trichrome staining images from day 28 after MI. Scale bar=1 mm. **E**, Quantification of cardiac scar areas from **D** on day 28 after MI (WT- AAV-Ctrl, ALDH2*2- AAV-Ctrl, WT- AAV-eIF3E KD, and ALDH2*2- AAV-eIF3E KD, n=6, 5, 7, and 6, per group). **F**, Fold changes in serum lactate dehydrogenase (LDH) activity levels. **G**, Oxidized phospholipids in the infarct tissues on day 3 after MI (n=5, 7, 6, and 6 per group). Upregulation, red; downregulation, blue. The color scale represents the *Z* score. **H** and **I**, TFRC (transferrin receptor), ACSL4 (acyl-coenzyme A synthetase long-chain family member 4), ALDH2 (acetaldehyde dehydrogenase 2), and eIF3E protein expression levels in infarct tissues on day 3 after MI (n=6, 6, 8, and 5 per group). Data are presented as mean±SEM. Data analyzed by mixed-effects ANOVA with Geisser-Greenhouse correction (**B** and **C**) and 2-way ANOVA (**E**, **F**, and **I**). AAV indicates adeno-associated virus; Echo, echocardiography; KD, knockdown; PC, phosphatidylcholine; and PE, phosphatidylethanolamine.

Fe^{2+} levels (Figure S14G) compared with ALDH2*2-AAV-control mice. Additionally, TFRC and ACSL4 protein levels were markedly reduced in ALDH2*2-eIF3E-KD hearts (Figure 6H and 6I), whereas mRNA levels were not altered (Figure S14H). Notably, these effects were genotype specific, as eIF3E-KD showed no impact in WT mice.

Taken together, these data suggest that ALDH2*2 exacerbates cardiac ischemic injury through eIF3E-mediated ferroptosis. Cardiomyocyte-specific eIF3E KD mitigates ferroptosis-driven damage, improving functional recovery in ALDH2*2 mice after MI.

DISCUSSION

This study shows that ferroptosis is involved in patients and mice carrying the ALDH2*2 variant. Mechanistically, we found that ALDH2 affects ferroptosis by competitively binding to the N-terminal two-thirds of eIF3E (within the eIF3 complex), competing with eIF4G1, and modulating the translation of critical proteins involved in ferroptosis. In ALDH2*2 cardiomyocytes under hypoxia, enhanced translation of specific genes containing the GAGGACR motif was observed, predominantly promoting cardiomyocyte ferroptosis. EIF3E KD or pharmacological inhibition of ferroptosis with Fer-1 effectively restored cardiac function in ALDH2*2 mice after ischemic AHF (Figure 7). This study underscores the critical role of the ALDH2*2 mutant in exacerbating AHF after MI through ferroptosis-linked mechanisms.

ALDH2*2 and Heart Failure After MI

Ischemia and reperfusion inflict distinct types of injury,[1] and clinical data show that ALDH2*2 carriers exhibit exacerbated ischemic damage induced by MI. However, the underlying mechanisms remain poorly defined. This association coincides with our findings that patients with ALDH2*2 AHF exhibit exacerbated oxidative stress, characterized by increased bioactive lipids derived from PUFAs, alongside decreased levels of CoQ10 and BH4, hallmarks of ferroptosis. Using the gold-standard method for in vivo lipid peroxidation assessment,[55] we observed significantly elevated levels of AA, 15d-PGD_2, and the mortality-predictive 14,15-DHET/14,15-epoxy eicosatetraenoic acid ratio in patients with ALDH2*2 AMI. These findings suggest that lipid peroxidation and dysregulated PUFA metabolism are central contributors to ferroptosis in ALDH2*2 carriers after MI. In ALDH2*2 mice after MI, Fer-1 pretreatment efficiently reduced AA levels (Figure 2I). However, we did not detect changes in CoQ9 or BH4 levels in cardiomyocytes, which warrants further investigation. It has been reported that ALDH2*2 carriers exhibit limited nitroglycerin bioactivation and that BH4 is a crucial cofactor for endothelial nitric oxide synthase activity.[56] Additionally, our previous study found that ALDH2 mutation or deficiency stabilizes 3-hydroxy-3-methylglutaryl-CoA reductase (HMGCR).[57] Because CoQ10 is downstream of HMGCR in cholesterol biosynthesis, and statins inhibit HMGCR activity, the relationship between ALDH2 deficiency, CoQ10, and HMGCR levels requires further exploration in other organs and cell types in patients and MI mouse models.

The majority of previous reports attributed the increased risks of CVD to the accumulation of alcohol-derived acetaldehydes or lipid aldehydes generated from lipid peroxidation (eg, 4-hydroxynonenal, 4-HNE). Studies also show that elevated circulating miR-34a after MI promotes cardiomyocyte apoptosis by suppressing ALDH2,[38] accounting for the decreased ALDH2 protein levels after MI. Consistent with this, activation of ALDH2 enzymatic activity, such as Alda-1, has been explored for the treatment of MI, especially for ALDH2*2 carriers.[35] Conceivably, decreased ALDH2 enzymatic function in ALDH2*2 can be either attributable to ALDH2 mutation or decreased ALDH2 levels, and several experimental studies have linked decreased ALDH2 enzyme function to heart failure with excessive alcohol intake. However, we and others have shown that the prevalence of alcohol drinking was obviously lower in ALDH2*2 carriers with heart failure (Table), suggesting unknown mechanisms underlying increased CVD risks in an alcohol-independent manner.

Cell Death Pathways in ALDH2*2

ALDH2*2 cardiomyocytes showed increased hypoxia-induced cell death, which can be rescued by inhibitors of ferroptosis (Fer-1), necroptosis (Nec-1), apoptosis (Z-VAD-FMK), iron overload (DFO), and autophagy (3-MA), indicating involvement of multiple death pathways (Figure S6B and S6C). Although autophagy drives ferroptosis in I/R by enhancing iron release,[58] FTH and NCOA4 levels showed no significant differences between the genotypes after MI (Figure S4E and S4F). In contrast, HMOX1 was significantly upregulated in ALDH2*2 infarct tissues, implying its greater role in iron release than

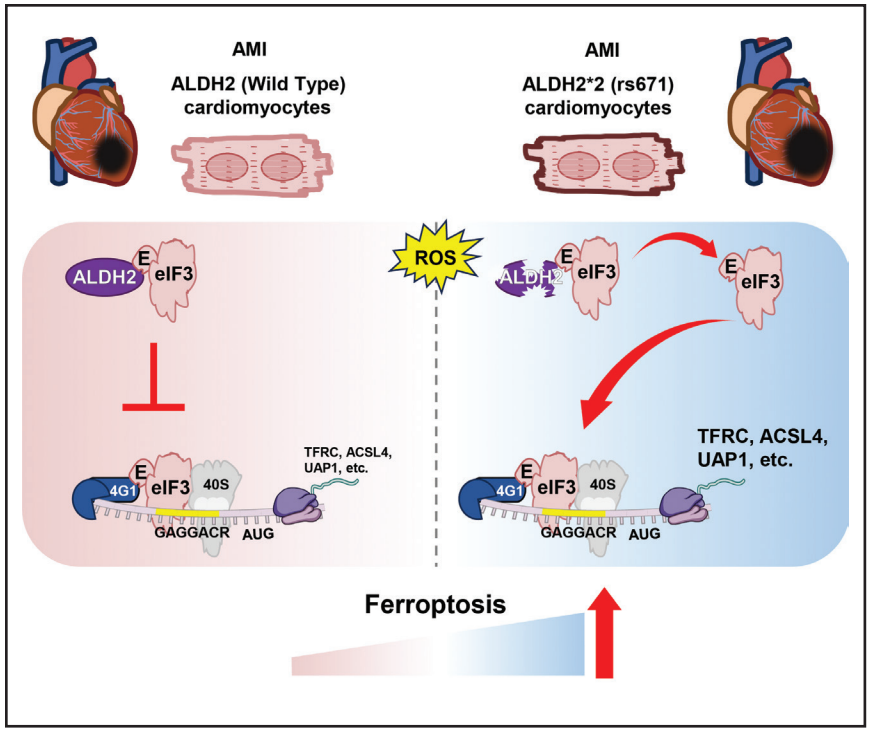

Figure 7. ALDH2 deficiency in ALDH2*2 predisposes cardiac cells to ferroptosis in heart failure.
ALDH2*2 facilitates ferroptosis-related protein translation through interaction with eIF3E to promote heart failure after myocardial infarction. **Left**, An ALDH2 (acetaldehyde dehydrogenase 2) wild-type heart after myocardial infarction. **Right**, An ALDH2*2 heart after myocardial infarction. The ALDH2*2 variant leads to ALDH2 deficiency, disrupting its interaction with the eIF3 complex by releasing the bound eIF3E. Moreover, released eIF3E recruits eIF4G1 and assembles an eIF3E-eIF4G1-mRNA ternary complex, driving the selective translation of mRNAs (eg, TFRC [transferrin receptor], ACSL4 (acyl-coenzyme A synthetase long-chain family member 4], and UAP1) containing the GAGGACR motif to promote ferroptosis. 40S indicates eukaryotic small ribosomal subunit; ALDH2*2, aldehyde dehydrogenase 2 rs671 mutant; AUG, the start codon; E, eukaryotic initiation factor 3 E; eIF3, eukaryotic initiation factor 3; eIF4G1, eukaryotic translation initiation factor 4 gamma 1; and MI, myocardial infarction.

ferritinophagy. As HMOX1 has dual functions (antioxidant/ferroptosis mediator)[59] and is constitutively elevated in ALDH2 deficiency,[60] this represents a promising novel pathway in ALDH2-related cardiac pathology that merits further exploration.

An established mechanism links ALOX15-driven ferroptosis (via 15-hydroperoxyeicosatetraenoic acid (15-HpETE)) to cardiac I/R injury.[61] We detected elevated ALOX15 products (13-HODE and 15-HETE) and their precursor AA in serum from ischemic ALDH2*2 mice (Figure 2I). Fer-1 treatment only fully reversed increased AA levels. This suggests that, although ALOX15-mediated ferroptosis contributes to ischemic injury, its role is modest in ALDH2 deficiency.

Lipidomic analyses revealed elevated levels of phospholipid species containing both nonoxygenated and oxygenated fatty acids in infarct tissues of ALDH2*2 mice. These mice exhibited worsened cardiac dysfunction after MI, alongside evidence of enhanced ferroptosis (increased iron, TFRC, and ACSL4), linking ferroptosis activity to cardiac injury.

Mechanisms of Ferroptosis in ALDH2*2 Ischemic Injury

Under hypoxia, ALDH2*2 myocytes exhibited markedly exacerbated global translation suppression (Figure 4I). Paradoxically, hypoxic ALDH2*2 cardiomyocytes selectively enhanced translation of GAGGACR motif–bearing transcripts (eg, ferroptosis-related genes *Tfrc* and *Acsl4*), leading to amplified redox imbalance and lipid peroxidation, which then reinforced suppression of bulk protein synthesis. In this study, we identified a novel mechanism by which ALDH2 interacts with the translation factor eIF3E to regulate the translation of critical proteins in ferroptosis. As extensively reported, the ALDH2*2 variant exhibits reduced levels of ALDH2 protein, which undergoes accelerated degradation with a shorter half-life,[62] impacting enzyme activity and protein expression. To explore this, we pretreated mice with the ALDH2 agonist Alda-1, the necroptosis inhibitor Nec-1, and the ferroptosis inhibitor Fer-1. The results showed that Alda-1 had no significant effect on LDH activity, whereas Nec-1 and Fer-1 exhibited protective effects on day 3 after MI (Figure 2G; Figure S3H). These data suggest that ALDH2 enzyme activity plays a limited role at this stage, and targeting ferroptosis may be a more effective strategy to reduce heart injury in ALDH2*2 mice after MI. Consistent with previous research that has linked 4-HNE in ALDH2 deficiency to iron accumulation in myocardial reperfusion-induced ferroptosis, our findings suggest that ALDH2 directly binds eIF3E, influencing the translation of TFRC (modulating iron) and ACSL4 (modulating PUFA-CoA), providing further insight into the underlying mechanisms for the role of ALDH2*2 in reperfusion injury and ferroptosis regulation.

Intriguingly, HIF-1α levels remained unchanged in hypoxia-induced ALDH2*2 cardiomyocytes (Figure S6D and S6E), contrasting with decreased levels in ALDH2*2 infarct tissue (Figure 3A through 3C). This discrepancy suggests that reduced HIF-1α levels in ALDH2*2 infarct tissues may occur in cardiac fibroblasts, potentially driving increased fibroblast proliferation, excessive scarring, and contractile dysfunction,[63] warranting further investigation.

Therapeutic Implications

We propose targeting cardiomyocyte ferroptosis as a therapeutic strategy for ALDH2*2 carriers to improve cardiac function after MI. Supporting this, cardiomyocyte-specific eIF3E KD reduced cardiac damage in mice, demonstrating that targeting the ALDH2/eIF3E axis offers a viable treatment approach for ALDH2*2-associated pathology. Interestingly, DFO, a US Food and Drug Administration–approved iron chelator, had a similar effect as Fer-1 in rescuing ALDH2*2 primary cardiac myocyte viability during hypoxia (Figure S6B). This suggests that iron metabolism plays a crucial role in hypoxia-induced cell death and lipid peroxidation in ALDH2*2. DFO is clinically used to treat iron overload conditions, such as those caused by chronic blood transfusions, hemochromatosis, or other disorders associated with excessive iron accumulation. Our study warrants further investigation to explore its clinical potential in treating ALDH2*2 patients in future research. Last, although our animal experiments were performed only in male mice, similar mechanisms likely operate in female mice and humans.

Overall, our study has identified ferroptosis as a key driver of MI in ALDH2*2 carriers, involving mediators like ACSL4 and TFRC. Targeting cardiomyocyte ferroptosis via cardiomyocyte-specific eIF3E KD or inhibition (Fer-1 and DFO) represents a novel approach for patients with ALDH2*2.

Conclusions

Our study demonstrates that ferroptosis contributes significantly to cardiomyocyte death and AHF in patients with ALDH2*2 after MI. Mechanistically, ALDH2 regulates ferroptosis by competitively binding to the N-terminal two-thirds of eIF3E (within the eIF3 complex), competing with eIF4G1, and modulating the translation of proteins, particularly those involved in ferroptosis. In ALDH2*2 cardiomyocytes under hypoxia, ALDH2 deficiency enhanced the translation of specific genes containing the GAG-GACR motif, promoting cardiomyocyte ferroptosis. EIF3E KD or pharmacological inhibition of ferroptosis with Fer-1 effectively restored cardiac function in ALDH2*2 mice after ischemic AHF. These findings suggest that targeting the ALDH2*2/eIF3E axis and ferroptosis may be an effective strategy for restoring cardiac function and treating heart failure induced by MI in ALDH2*2 carriers.

ARTICLE INFORMATION

Received April 24, 2025; accepted September 29, 2025.

Affiliations

CAS Key Laboratory of Nutrition, Metabolism and Food Safety, Shanghai Institute of Nutrition and Health, University of Chinese Academy of Sciences, Chinese Academy of Sciences, Shanghai, China (X.C., R.L., X.X., N.L., L.Z., L.L., H.M., Y.W., C.Y., S.C., H.-T.Y.). CAS Key Laboratory of Tissue Microenvironment and Tumor, Laboratory of Molecular Cardiology, Shanghai Institute of Nutrition and Health, University of Chinese Academy of Sciences, Shanghai, China (X.Y., P.S., H.Y.). Department of Biomedical Sciences, College of Biomedicine, Institute of Digital Medicine, Tung Biomedical Science Center, State Key Laboratory of Marine Environmental Health (SKLMEH), The Shenzhen Research Institute and Futian Research Institute, City University of Hong Kong, Hong Kong, China (S.Z., H.Y.). School of Life Science and Technology, ShanghaiTech University, Shanghai, China (R.L., C.Y., H.Y.). Department of Cardiology, Naval Medical University, Shanghai, China (J.Z., M.Z., T.L., P.L.). Frontier Medical Center, Tianfu Jincheng Laboratory, Chengdu, Sichuan, China (Y.W.). Bio-med Big Data Center, CAS Key Laboratory of Computational Biology, CAS Center for Excellence in Molecular Cell Science, Shanghai Institute of Nutrition and Health, University of Chinese Academy of Sciences, Shanghai, China (Y.Y.). Department of Cardiology, Second Affiliated Hospital of Harbin Medical University, Key Laboratory of Myocardial Ischemia, Chinese Ministry of Education, Harbin, China (J.T.). Department of Cardiology, Zhongshan Hospital, Fudan University, Shanghai Institute of Cardiovascular Diseases, Shanghai, China (A.S.). Institutes of Biomedical Sciences, Fudan University, Shanghai, China (A.S.). Department of Endocrinology, Shenzhen Second People's Hospital, the First Affiliated Hospital of Shenzhen University, Health Science Center of Shenzhen University, Shenzhen Clinical Research Center for Metabolic Diseases, Shenzhen Center for Diabetes Control and Prevention, Shenzhen, Guangdong Province, China (W.W., D.Y.). Department of Cardiology, The Eighth Affiliated Hospital, Joint Laboratory of Guangdong-Hong Kong-Macao Universities for Nutritional Metabolism and Precise Prevention and Control of Major Chronic Diseases, Sun Yat-sen University, Shenzhen, China (H.H.).

Acknowledgments

The authors thank APExBIO (Shanghai, China) for ribosome profiling library preparation, sequencing, and bioinformatic analysis. The authors also thank the Mass Spectrometry/Molecular Biology/Biochemistry/Cell Technology/Experimental Animal/Biological Sample Pathology Analysis Platform at Shanghai Institute of Nutrition and Health, Chinese Academy of Sciences.

Author Contributions

Dr H. Yin and Dr X. Chen conceived the idea for the study. Dr H. Yin, Dr P. Li, Dr Huang, Dr Yang, Dr Tian, Dr Sun, Dr Wang, Dr Yan, Dr X. Chen, Dr Yu, Dr Zhong, Dr Sha, Dr Xu, Dr L. Li, Dr Liang, and Dr L. Zhang were responsible for developing the study design. Dr P. Li, Dr X. Chen, Dr Yu, Dr Sha, Dr R. Li, Dr Xu, Dr Liang, Dr L. Zhang, Dr L. Li, Dr J. Zhang, Dr Zhou, Dr Lv, Dr Ma, Dr Wang, Dr Ye, Dr C. Yin, Dr S. Chen, and Dr Yang supervised the data collection process and managed participant recruitment. Dr X. Chen, Dr Yu, Dr Sha, Dr R. Li, Dr Xu, Dr Liang, Dr L. Zhang, Dr L. Li, Dr J. Zhang, Dr Zhou, Dr Lv, Dr Ma, Dr Wang, Dr Ye, Dr C. Yin, and Dr S. Chen contributed to method development and data analysis. Dr H. Yin, Dr P. Li, Dr Huang, Dr X. Chen, Dr Zhong, Dr Tian, Dr Sun, Dr Wang, and Dr Yan drafted and revised the manuscript. All authors critically reviewed the article, provided feedback, and approved the final version for submission. Dr H. Yin is the guarantor of the study.

Sources of Funding

This research was funded by grants from the National Natural Science Foundation of China (32030053 and 32241017), the National Key Research and Development Program of China (2022YFC2503300), the Shenzhen Medical Research Fund (SMRF B2302042), and the RGC General Research Fund (9043653); startup funds from the City University of Hong Kong (9380154), the RGC Theme-based Research Scheme (8770011), and the TBSC Project fund and Futian research project (9609327). Dr Yang was supported by an NSFC grant (82170293). Dr. Hui Huang was supported by NSFC (82330021) and Shenzhen Science and Technology Program (ZDSYS 20220606100801004). Dr Yan was supported by the Shenzhen Clinical Research Center for Metabolic Diseases (Shenzhen Science, Technology and Innovation [2021]287) and the Shenzhen Center for Diabetes Control and Prevention (SZMHC [2020]46). Open Access was made possible with partial support from the Open Access Publishing Fund of the City University of Hong Kong.

Disclosures

None.

Supplemental Material

Supplemental Methods
Tables S1–S5
Figure S1–S14
References 64–75

REFERENCES

1. Heusch G. Myocardial ischaemia-reperfusion injury and cardioprotection in perspective. *Nat Rev Cardiol.* 2020;17:773–789. doi: 10.1038/s41569-020-0403-y

2. GBD 2016 Causes of Death Collaborators. Global, regional, and national age-sex specific mortality for 264 causes of death, 1980-2016: a systematic analysis for the Global Burden of Disease Study 2016. *Lancet*. 2017;390:1151–1210. doi: 10.1016/S0140-6736(17)32152-9
3. The top 10 causes of death. *World Health Organization*. Accessed July 15, 2024. https://www.who.int/news-room/fact-sheets/detail/the-top-10-causes-of-death
4. Davidson SM, Adameová A, Barile L, Cabrera-Fuentes HA, Lazou A, Pagliaro P, Stensløkken KO, Garcia-Dorado D; EU-CARDIOPROTECTION COST Action (CA16225). Mitochondrial and mitochondrial-independent pathways of myocardial cell death during ischaemia and reperfusion injury. *J Cell Mol Med*. 2020;24:3795–3806. doi: 10.1111/jcmm.15127
5. Du B, Fu Q, Yang Q, Yang Y, Li R, Yang X, Yang Q, Li S, Tian J, Liu H. Different types of cell death and their interactions in myocardial ischemia-reperfusion injury. *Cell Death Discov*. 2025;11:87. doi: 10.1038/s41420-025-02372-5
6. Xiang Q, Yi X, Zhu XH, Wei X, Jiang DS. Regulated cell death in myocardial ischemia–reperfusion injury. *Trends Endocrinol Metab*. 2024;35:219–234. doi: 10.1016/j.tem.2023.10.010
7. Dixon SJ, Lemberg KM, Lamprecht MR, Skouta R, Zaitsev EM, Gleason CE, Patel DN, Bauer AJ, Cantley AM, Yang WS, et al. Ferroptosis: an iron-dependent form of nonapoptotic cell death. *Cell*. 2012;149:1060–1072. doi: 10.1016/j.cell.2012.03.042
8. Feng H, Schorpp K, Jin J, Yozwiak CE, Hoffstrom BG, Decker AM, Rajbhandari P, Stokes ME, Bender HG, Csuka JM, et al. Transferrin receptor is a specific ferroptosis marker. *Cell Rep*. 2020;30:3411–3423.e7. doi: 10.1016/j.celrep.2020.02.049
9. Dixon SJ, Olzmann JA. The cell biology of ferroptosis. *Nat Rev Mol Cell Biol*. 2024;25:424–442. doi: 10.1038/s41580-024-00703-5
10. Dai E, Chen X, Linkermann A, Jiang X, Kang R, Kagan VE, Bayir H, Yang WS, Garcia-Saez AJ, Ioannou MS, et al. A guideline on the molecular ecosystem regulating ferroptosis. *Nat Cell Biol*. 2024;26:1447–1457. doi: 10.1038/s41556-024-01360-8
11. Doll S, Proneth B, Tyurina YY, Panzilius E, Kobayashi S, Ingold I, Irmler M, Beckers J, Aichler M, Walch A, et al. ACSL4 dictates ferroptosis sensitivity by shaping cellular lipid composition. *Nat Chem Biol*. 2016;13:91–98. doi: 10.1038/nchembio.2239
12. Friedmann Angeli JP, Krysko DV, Conrad M. Ferroptosis at the crossroads of cancer-acquired drug resistance and immune evasion. *Nat Rev Cancer*. 2019;19:405–414. doi: 10.1038/s41568-019-0149-1
13. Fang X, Ardehali H, Min J, Wang F. The molecular and metabolic landscape of iron and ferroptosis in cardiovascular disease. *Nat Rev Cardiol*. 2022;20:7–23. doi: 10.1038/s41569-022-00735-4
14. Chen CH, Ferreira JCB, Mochly-Rosen D. ALDH2 and cardiovascular disease. *Adv Exp Med Biol*. 2019;1193:53–67. doi: 10.1007/978-981-13-6260-6_3
15. Zhang J, Guo Y, Zhao X, Pang J, Pan C, Wang J, Wei S, Yu X, Zhang C, Chen Y, et al. The role of aldehyde dehydrogenase 2 in cardiovascular disease. *Nat Rev Cardiol*. 2023;20:495–509. doi: 10.1038/s41569-023-00839-5
16. von Scheidt M, Zhao Y, Kurt Z, Pan C, Zeng L, Yang X, Schunkert H, Lusis AJ. Applications and limitations of mouse models for understanding human atherosclerosis. *Cell Metab*. 2017;25:248–261. doi: 10.1016/j.cmet.2016.11.001
17. Wang LJ, Yu HY, Gao W. Association of Aldh2 gene polymorphism with cardiac function insufficiency after myocardial infarction in Chinese Han population. *Circulation*. 2019;140(suppl I). doi: 10.1161/circ.140.suppl_1.12754.
18. Ueta CB, Campos JC, Albuquerque RPE, Lima VM, Disatnik MH, Sanchez AB, Chen CH, de Medeiros MHG, Yang W, Mochly-Rosen D, et al. Cardioprotection induced by a brief exposure to acetaldehyde: role of aldehyde dehydrogenase 2. *Cardiovasc Res*. 2018;114:1006–1015. doi: 10.1093/cvr/cvy070
19. Zhong S, Li L, Zhang YL, Zhang L, Lu J, Guo S, Liang N, Ge J, Zhu M, Tao Y, et al. Acetaldehyde dehydrogenase 2 interactions with LDLR and AMPK regulate foam cell formation. *J Clin Invest*. 2019;129:252–267. doi: 10.1172/JCI122064
20. Li L, Zhong S, Li R, Liang N, Zhang L, Xia S, Xu X, Chen X, Chen S, Tao Y, et al. Aldehyde dehydrogenase 2 and PARP1 interaction modulates hepatic HDL biogenesis by LXRalpha-mediated ABCA1 expression. *JCI Insight*. 2022;7:e155869. doi: 10.1172/jci.insight.155869
21. Chen X, Li X, Xu X, Li L, Liang N, Zhang L, Lv J, Wu Y-C, Yin H. Ferroptosis and cardiovascular disease: role of free radical-induced lipid peroxidation. *Free Radic Res*. 2021;55:405–415. doi: 10.1080/10715762.2021.1876856
22. Liu L, Pang J, Qin D, Li R, Zou D, Chi K, Wu W, Rui H, Yu H, Zhu W, et al. Deubiquitinase OTUD5 as a novel protector against 4-HNE-triggered ferroptosis in myocardial ischemia/reperfusion injury. *Adv Sci (Weinh)*. 2023;10:e2301852. doi: 10.1002/advs.202301852
23. Jin S, Chen J, Chen L, Histen G, Lin Z, Gross S, Hixon J, Chen Y, Kung C, Chen Y, et al. ALDH2(E487K) mutation increases protein turnover and promotes murine hepatocarcinogenesis. *Proc Natl Acad Sci U S A*. 2015;112:9088–9093. doi: 10.1073/pnas.1510757112
24. Heidenreich PA, Bozkurt B, Aguilar D, Allen LA, Byun JJ, Colvin MM, Deswal A, Drazner MH, Dunlay SM, Evers LR, et al; ACC/AHA Joint Committee Members. 2022 AHA/ACC/HFSA Guideline for the Management of Heart Failure: A report of the American College of Cardiology/American Heart Association Joint Committee on Clinical Practice Guidelines. *Circulation*. 2022;145:e895–e1032. doi: 10.1161/CIR.0000000000001063
25. Lamb RJ, Griffiths K, Lip GYH, Sorokin V, Frenneaux MP, Feelisch M, Madhani M. ALDH2 polymorphism and myocardial infarction: from alcohol metabolism to redox regulation. *Pharmacol Ther*. 2024;259:108666. doi: 10.1016/j.pharmthera.2024.108666
26. Galy B, Conrad M, Muckenthaler M. Mechanisms controlling cellular and systemic iron homeostasis. *Nat Rev Mol Cell Biol*. 2023;25:133–155. doi: 10.1038/s41580-023-00648-1
27. Yin H, Zhou Y, Zhu M, Hou S, Li Z, Zhong H, Lu J, Meng T, Wang J, Xia L, et al. Role of mitochondria in programmed cell death mediated by arachidonic acid-derived eicosanoids. *Mitochondrion*. 2013;13:209–224. doi: 10.1016/j.mito.2012.10.003
28. Ma K, Yang J, Shao Y, Li P, Guo H, Wu J, Zhu Y, Zhang H, Zhang X, Du J, et al. Therapeutic and prognostic significance of arachidonic acid in heart failure. *Circ Res*. 2022;130:1056–1071. doi: 10.1161/CIRCRESAHA.121.320548
29. Raizner AE, Quiñones MA. Coenzyme Q(10) for patients with cardiovascular disease: JACC Focus Seminar. *J Am Coll Cardiol*. 2021;77:609–619. doi: 10.1016/j.jacc.2020.12.009
30. Prabhu SD, Frangogiannis NG. The biological basis for cardiac repair after myocardial infarction: from inflammation to fibrosis. *Circ Res*. 2016;119:91–112. doi: 10.1161/CIRCRESAHA.116.303577
31. Weindel CG, Martinez EL, Zhao X, Mabry CJ, Bell SL, Vail KJ, Coleman AK, VanPortfliet JJ, Zhao B, Wagner AR, et al. Mitochondrial ROS promotes susceptibility to infection via gasdermin D-mediated necroptosis. *Cell*. 2022;185:3214–3231.e23. doi: 10.1016/j.cell.2022.06.038
32. Syeda JN, Rutkofsky IH, Muhammad AS, Balla Abdalla TH, Saghir Z. The psycho-cardiac coupling, myocardial remodeling, and neuroendocrine factor levels: the psychosomatics of major depressive disorder. *Cureus*. 2018;10:e2464. doi: 10.7759/cureus.2464
33. Placidi M, Di Emidio G, Virmani A, D'Alfonso A, Artini PG, D'Alessandro AM, Tatone C. Carnitines as mitochondrial modulators of oocyte and embryo bioenergetics. *Antioxidants*. 2022;11:745. doi: 10.3390/antiox11040745
34. Li W, Feng G, Gauthier JM, Lokshina I, Higashikubo R, Evans S, Liu X, Hassan A, Tanaka S, Cicka M, et al. Ferroptotic cell death and TLR4/Trif signaling initiate neutrophil recruitment after heart transplantation. *J Clin Invest*. 2019;129:2293–2304. doi: 10.1172/JCI126428
35. Chen CH, Budas GR, Churchill EN, Disatnik MH, Hurley TD, Mochly-Rosen D. Activation of aldehyde dehydrogenase-2 reduces ischemic damage to the heart. *Science*. 2008;321:1493–1495. doi: 10.1126/science.1158554
36. Friedmann Angeli JP, Schneider M, Proneth B, Tyurina YY, Tyurin VA, Hammond VJ, Herbach N, Aichler M, Walch A, Eggenhofer E, et al. Inactivation of the ferroptosis regulator Gpx4 triggers acute renal failure in mice. *Nat Cell Biol*. 2014;16:1180–1191. doi: 10.1038/ncb3064
37. Li W, Xiang Z, Xing Y, Li S, Shi S. Mitochondria bridge HIF signaling and ferroptosis blockage in acute kidney injury. *Cell Death Dis*. 2022;13:308. doi: 10.1038/s41419-022-04770-4
38. Kiyuna LA, Candido DS, Bechara LRG, Jesus ICG, Ramalho LS, Krum B, Albuquerque RP, Campos JC, Bozi LHM, Zambelli VO, et al. 4-Hydroxynonenal impairs miRNA maturation in heart failure via Dicer post-translational modification. *Eur Heart J*. 2023;44:4696–4712. doi: 10.1093/eurheartj/ehad662
39. Conrad M, Pratt DA. The chemical basis of ferroptosis. *Nat Chem Biol*. 2019;15:1137–1147. doi: 10.1038/s41589-019-0408-1
40. Mancias JD, Wang X, Gygi SP, Harper JW, Kimmelman AC. Quantitative proteomics identifies NCOA4 as the cargo receptor mediating ferritinophagy. *Nature*. 2014;509:105–109. doi: 10.1038/nature13148
41. Fang X, Cai Z, Wang H, Han D, Cheng Q, Zhang P, Gao F, Yu Y, Song Z, Wu Q, et al. Loss of cardiac ferritin H facilitates cardiomyopathy via Slc7a11-mediated ferroptosis. *Circ Res*. 2020;127:486–501. doi: 10.1161/CIRCRESAHA.120.316509
42. Hassannia B, Wiernicki B, Ingold I, Qu F, Van Herck S, Tyurina YY, Bayır H, Abhari BA, Angeli JPF, Choi SM, et al. Nano-targeted induction of dual ferroptotic mechanisms eradicates high-risk neuroblastoma. *J Clin Invest*. 2018;128:3341–3355. doi: 10.1172/JCI99032

43. Zhu ZY, Liu YD, Gong Y, Jin W, Topchiy E, Turdi S, Gao YF, Culver B, Wang SY, Ge W, et al. Mitochondrial aldehyde dehydrogenase (ALDH2) rescues cardiac contractile dysfunction in an APP/PS1 murine model of Alzheimer's disease via inhibition of ACSL4-dependent ferroptosis. *Acta Pharmacol Sin*. 2021;43:39–49. doi: 10.1038/s41401-021-00635-2
44. Fan F, Sun A, Zhao H, Liu X, Zhang W, Jin X, Wang C, Ma X, Shen C, Zou Y, et al. MicroRNA-34a promotes cardiomyocyte apoptosis post myocardial infarction through down-regulating aldehyde dehydrogenase 2. *Curr Pharm Des*. 2013;19:4865–4873. doi: 10.2174/1381612811319990325
45. Zhai X, Wang W, Sun S, Han Y, Li J, Cao S, Li R, Xu T, Yuan Q, Wang J, et al. 4-Hydroxy-2-nonenal promotes cardiomyocyte necroptosis via stabilizing receptor-interacting serine/threonine-protein kinase 1. *Front Cell Dev Biol*. 2021;9:721795. doi: 10.3389/fcell.2021.721795
46. Ma H, Guo R, Yu L, Zhang Y, Ren J. Aldehyde dehydrogenase 2 (ALDH2) rescues myocardial ischaemia/reperfusion injury: role of autophagy paradox and toxic aldehyde. *Eur Heart J*. 2011;32:1025–1038. doi: 10.1093/eurheartj/ehq253
47. Snieckute G, Ryder L, Vind AC, Wu Z, Arendrup FS, Stoneley M, Chamois S, Martinez-Val A, Leleu M, Dreos R, et al. ROS-induced ribosome impairment underlies ZAKalpha-mediated metabolic decline in obesity and aging. *Science*. 2023;382:eadf3208. doi: 10.1126/science.adf3208
48. Gross JD, Moerke NJ, von der Haar T, Lugovskoy AA, Sachs AB, McCarthy JE, Wagner G. Ribosome loading onto the mRNA cap is driven by conformational coupling between eIF4G and eIF4E. *Cell*. 2003;115:739–750. doi: 10.1016/s0092-8674(03)00975-9
49. Duan H, Zhang S, Zarai Y, Öllinger R, Wu Y, Sun L, Hu C, He Y, Tian G, Rad R, et al. eIF3 mRNA selectivity profiling reveals eIF3k as a cancer-relevant regulator of ribosome content. *EMBO J*. 2023;42:e112362. doi: 10.15252/embj.2022112362
50. Lee A, Kranzusch P, Cate J. eIF3 targets cell-proliferation messenger RNAs for translational activation or repression. *Nature*. 2015;522:111–114. doi: 10.1038/nature14267
51. Lin Y, Li F, Huang L, Polte C, Duan H, Fang J, Sun L, Xing X, Tian G, Cheng Y, et al. eIF3 Associates with 80S ribosomes to promote translation elongation, mitochondrial homeostasis, and muscle health. *Mol Cell*. 2020;79:575–587.e7. doi: 10.1016/j.molcel.2020.06.003
52. LeFebvre AK, Korneeva NL, Trutschl M, Cvek U, Duzan RD, Bradley CA, Hershey JW, Rhoads RE. Translation initiation factor eIF4G-1 binds to eIF3 through the eIF3e subunit. *J Biol Chem*. 2006;281:22917–22932. doi: 10.1074/jbc.M605418200
53. Brito Querido J, Díaz-López I, Ramakrishnan V. The molecular basis of translation initiation and its regulation in eukaryotes. *Nat Rev Mol Cell Biol*. 2024;25:168–186. doi: 10.1038/s41580-023-00624-9
54. Shah M, Su D, Scheliga JS, Pluskal T, Boronat S, Motamedchaboki K, Campos AR, Qi F, Hidalgo E, Yanagida M, et al. A transcript-specific eIF3 complex mediates global translational control of energy metabolism. *Cell Rep*. 2016;16:1891–1902. doi: 10.1016/j.celrep.2016.07.006
55. Murphy MP, Bayir H, Belousov V, Chang CJ, Davies KJA, Davies MJ, Dick TP, Finkel T, Forman HJ, Janssen-Heininger Y, et al. Guidelines for measuring reactive oxygen species and oxidative damage in cells and in vivo. *Nat Metab*. 2022;4:651–662. doi: 10.1038/s42255-022-00591-z
56. Fanet H, Capuron L, Castanon N, Calon F, Vancassel S. Tetrahydrobioterin (BH4) Pathway: From Metabolism to Neuropsychiatry. *Curr Neuropharmacol*. 2021;19:591–609. doi: 10.2174/1570159X18666200729103529
57. Zhong S, Li L, Liang N, Zhang L, Xu X, Chen S, Yin H. Acetaldehyde Dehydrogenase 2 regulates HMG-CoA reductase stability and cholesterol synthesis in the liver. *Redox Biol*. 2021;41:101919. doi: 10.1016/j.redox.2021.101919
58. Wang X, Chen T, Chen S, Zhang J, Cai L, Liu C, Zhang Y, Wu X, Li N, Ma Z, et al. STING aggravates ferroptosis-dependent myocardial ischemia-reperfusion injury by targeting GPX4 for autophagic degradation. *Signal Transduct Target Ther*. 2025;10:136. doi: 10.1038/s41392-025-02216-9
59. Conrad M, Proneth B. Broken hearts: Iron overload, ferroptosis and cardiomyopathy. *Cell Res*. 2019;29:263–264. doi: 10.1038/s41422-019-0150-y
60. Matsumoto A, Thompson D, Chen Y, Vasiliou V, Kawamoto T, Ichiba M. Heme oxygenase 1 protects ethanol-administered liver tissue in Aldh2 knockout mice. *Alcohol*. 2016;52:49–54. doi: 10.1016/j.alcohol.2016.02.004
61. Cai W, Liu L, Shi X, Liu Y, Wang J, Fang X, Chen Z, Ai D, Zhu Y, Zhang X. Alox15/15-HpETE aggravates myocardial ischemia-reperfusion injury by promoting cardiomyocyte ferroptosis. *Circulation*. 2023;147:1444–1460. doi: 10.1161/CIRCULATIONAHA.122.060257
62. Larson HN, Weiner H, Hurley TD. Disruption of the coenzyme binding site and dimer interface revealed in the crystal structure of mitochondrial aldehyde dehydrogenase "Asian" variant. *J Biol Chem*. 2005;280:30550–30556. doi: 10.1074/jbc.M502345200
63. Janbandhu V, Tallapragada V, Patrick R, Li Y, Abeygunawardena D, Humphreys DT, Martin EMMA, Ward AO, Contreras O, Farbehi N, et al. Hif-1a suppresses ROS-induced proliferation of cardiac fibroblasts following myocardial infarction. *Cell Stem Cell*. 2022;29:281–297.e12. doi: 10.1016/j.stem.2021.10.009
64. Song K Nam YJ, Luo X, Qi X, Tan W, Huang GN, Acharya A, Smith CL, Tallquist MD, Neilson EG, et al. Heart repair by reprogramming non-myocytes with cardiac transcription factors. *Nature*. 2012;485:599–604. doi: 10.1038/nature11139
65. Lu J, Chen B, Chen T, Guo S, Xue X, Chen Q, Zhao M, Xia L, Zhu Z, Zheng L, et al. Comprehensive metabolomics identified lipid peroxidation as a prominent feature in human plasma of patients with coronary heart diseases. *Redox Biol*. 2017;12:899–907. doi: 10.1016/j.redox.2017.04.032
66. Doll S, Freitas FP, Shah R, Aldrovandi M, da Silva MC, Ingold I, Goya Grocin A, Xavier da Silva TN, Panzilius E, Scheel CH, et al. FSP1 is a glutathione-independent ferroptosis suppressor. *Nature*. 2019;575:693–698. doi: 10.1038/s41586-019-1707-0
67. Wang W, Green M, Choi JE, Gijón M, Kennedy PD, Johnson JK, Liao P, Lang X, Kryczek I, Sell A, et al. CD8(+) T cells regulate tumour ferroptosis during cancer immunotherapy. *Nature*. 2019;569:270–274. doi: 10.1038/s41586-019-1170-y
68. Wang B, Wu L, Chen J, Dong L, Chen C, Wen Z, Hu J, Fleming I, Wang DW. Metabolism pathways of arachidonic acids: mechanisms and potential therapeutic targets. *Signal Transduct Target Ther*. 2021;6:94. doi: 10.1038/s41392-020-00443-w
69. Liu G, Sun L, Pan A, Zhu M, Li Z, Wang Z, Liu X, Ye X, Li H, Zheng H, et al. Nickel exposure is associated with the prevalence of type 2 diabetes in Chinese adults. *Int J Epidemiol*. 2015;44:240–248. doi: 10.1093/ije/dyu200
70. Cronin SJF, Rao S, Tejada MA, Turnes BL, Licht-Mayer S, Omura T, Brenneis C, Jacobs E, Barrett L, Latremoliere A, et al. Phenotypic drug screen uncovers the metabolic GCH1/BH4 pathway as key regulator of EGFR/KRAS-mediated neuropathic pain and lung cancer. *Sci Transl Med*. 2022;14:eabj1531. doi: 10.1126/scitranslmed.abj1531
71. Guo H, Yu X, Liu Y, Paik DT, Justesen JM, Chandy M, Jahng JWS, Zhang T, Wu W, Rwere F, et al. SGLT2 inhibitor ameliorates endothelial dysfunction associated with the common ALDH2 alcohol flushing variant. *Sci Transl Med*. 2023;15:eabp9952. doi: 10.1126/scitranslmed.abp9952
72. Han C, Sun L, Pan Q, Sun Y, Wang W, Chen Y. Polysome profiling followed by quantitative PCR for identifying potential micropeptide encoding long non-coding RNAs in suspension cell lines. *STAR Protoc*. 2022;3:101037. doi: 10.1016/j.xpro.2021.101037
73. Ye Y, Wang Z, Yang Y. Comprehensive identification of translatable circular RNAs using polysome profiling. *Bio Protoc*. 2021;11:e4167. doi: 10.21769/BioProtoc.4167
74. Yang H, Zingaro VA, Lincoff J, Tom H, Oikawa S, Oses-Prieto JA, Edmondson Q, Seiple I, Shah H, Kajimura S, et al. Remodelling of the translatome controls diet and its impact on tumorigenesis. *Nature*. 2024;633:189–197. doi: 10.1038/s41586-024-07781-7
75. Loayza-Puch F, Rooijers K, Buil LC, Zijlstra J, Oude Vrielink JF, Lopes R, Ugalde AP, van Breugel P, Hofland I, Wesseling J, et al. Tumour-specific proline vulnerability uncovered by differential ribosome codon reading. *Nature*. 2016;530:490–494. doi: 10.1038/nature16982